HHS Public Access

Author manuscript

J Immunol. Author manuscript; available in PMC 2020 August 01.

Published in final edited form as:

J Immunol. 2019 August 01; 203(3): 607–626. doi:10.4049/jimmunol.1801252.

Critical Roles for Coiled-coil Dimers of Butyrophilin 3A1 in the Sensing of Prenyl Pyrophosphates by Human Vγ2Vδ2 T Cells

Hong Wang[*,†], **Mohanad H. Nada**[*,†,‡,1], **Yoshimasa Tanaka**[§,¶], **Shun Sakuraba**[‖,2], **Craig T. Morita**[*,†,#]

[*]Division of Immunology, Department of Internal Medicine, University of Iowa Carver College of Medicine, Iowa City, IA 52242

[†]Department of Veterans Affairs, Iowa City Health Care System, Iowa City, IA 52246

[‡]College of Medicine, Tikrit University, Tiktit, Iraq, 34001

[§]Center for Bioinformatics and Molecular Medicine, Graduate School of Biomedical Sciences, Nagasaki University, 1-12-4 Sakamoto, Nagasaki 852-8523, Japan

[¶]Hyogo College of Medicine, 1-1 Mukogawa, Nishinomiya, Hyogo 663-8501, Japan

[‖]Graduate School of Frontier Sciences, The University of Tokyo, Kashiwa, Chiba 277-8561, Japan

[#]Interdisciplinary Graduate Program in Immunology, University of Iowa Carver College of Medicine, Iowa City, IA 52242

Abstract

Vγ2Vδ2 T cells play important roles in human immunity to pathogens and tumors. Their TCRs respond to the sensing of isoprenoid metabolites, such as (*E*)-4-hydroxy-3-methyl-but-2-enyl pyrophosphate and isopentenyl pyrophosphate, by butyrophilin (BTN) 3A1. BTN3A1 is an Ig superfamily protein with extracellular IgV/IgC domains and intracellular B30.2 domains that bind prenyl pyrophosphates. We have proposed that intracellular α helices form a coiled-coil dimer that functions as a spacer for the B30.2 domains. To test this, five pairs of anchor residues were mutated to glycine to destabilize the coiled-coil dimer. Despite maintaining surface expression, BTN3A1 mutagenesis either abrogated or decreased stimulation by (*E*)-4-hydroxy-3-methyl-but-2-enyl pyrophosphate. BTN3A2 and BTN3A3 proteins and orthologs in alpacas and dolphins are also predicted to have similar coiled-coil dimers. A second short coiled-coil region dimerizes the B30.2 domains. Molecular dynamics simulations predict that mutation of a conserved tryptophan residue in this region will destabilize the dimer, explaining the loss of stimulation by BTN3A1 proteins with this mutation. The juxtamembrane regions of other BTN/BTN-like

Address correspondence and reprint requests to Craig T. Morita, M.D., Ph.D., Division of Immunology, Department of Internal Medicine, University of Iowa, Iowa City Veterans Affairs Health Care System, 601 Highway 6 West, Research (151), Iowa City, IA 52246. Craig-Morita@uiowa.edu, Phone (319) 338-0581 Ext. 7608; Fax (319) 339-7162.

[1]Current address: The American University of Iraq, Sulaimani (AUIS), Sulaymaniah, Iraq, 46001

[2]Current address: Quantum Beam Science Research Directorate, National Institutes for Quantum and Radiological Research, Kyoto 619-0215, Japan

The online version of this article contains supplemental material.

Disclosures

C.T.M. is a co-inventor of U.S. Patent 8,012,466 on the development of live bacterial vaccines for activating γδ T cells. The other authors have no financial conflicts of interest.

proteins with B30.2 domains are similarly predicted to assume α helices, with many predicted to form coiled-coil dimers. An exon at the end of this region and the exon encoding the dimerization region for B30.2 domains are highly conserved. We propose that coiled-coil dimers function as rod-like helical molecular spacers to position B30.2 domains, as interaction sites for other proteins, and as dimerization regions to allow sensing by B30.2 domains. In these ways, the coiled-coil domains of BTN3A1 play critical roles for its function.

Keywords

human; gamma delta T cell; Vγ2Vδ2 T cells; butyrophilin 3A1; prenyl pyrophosphates; isopentenyl pyrophosphate; antigen presentation; isoprenoid metabolism

Introduction

T cells expressing γδ TCRs are unconventional T cells that have unique roles that bridge innate and adaptive immunity (1). In humans, γδ T cells play important roles in immunity to microbes and tumors. During certain bacterial and parasitic infections, γδ T cells expressing Vγ2Vδ2 TCRs can expand to up to half of circulating T cells (reviewed in 1). All of these Vγ2Vδ2 T cells respond to the microbial-specific isoprenoid metabolite (*E*)-4-hydroxy-3-methyl-but-2-enyl pyrophosphate (HMBPP) in the 2-*C*-methyl-D-erythritol 4-phosphate pathway for isoprenoid biosynthesis (2, 3). Vγ2Vδ2 T cells secrete inflammatory cytokines, such as IFN-γ and TNF-α, kill infected cells by secretion of perforin and granzymes, and kill released bacteria and parasites by granulolysin (4) and antimicrobial peptides (5, 6). This helps to protect humans and other primates from infection, as proven by the reduction in the number of *Mycobacterium tuberculosis* bacteria upon adoptive transfer of Vγ2Vδ2 T cells in monkeys (7).

Vγ2Vδ2 T cells also contribute to tumor immunity. Vγ2Vδ2 T cells kill all human tumor cell types that have been treated with aminobisphosphonates (1, 8–10). Treatment of lymphoma patients with pamidronate and IL-2 resulted in expansion of Vγ2Vδ2 T cells and partial remissions in several patients (11). Adoptive immunotherapy with Vγ2Vδ2 T cells has resulted in several partial and a few complete remissions in patients with solid tumors (12, 13), stable disease in patients with metastatic lung cancer (14–16), and slowed progression in patients with renal cell carcinoma (17).

In cancer therapy, Vγ2Vδ2 T cells respond to the accumulation of endogenous isopentenyl pyrophosphate (IPP) (18). This accumulation can be brought about by either pharmacological inhibition of farnesyl diphosphate synthase, using aminobisphosphonates (19–22), aminobisphosphonate prodrugs (10), or by small interfering RNA (siRNA)/short hairpin RNA (shRNA)-induced downregulation of its mRNA (22, 23). Stimulation by both direct (exogenous HMBPP or IPP) and indirect [aminobisphosphonate, alkylamine, or siRNA/shRNA inhibition of farnesyl diphosphate synthase (22)] stimuli is dependent on the Vγ2Vδ2 TCR (24, 25). Critical TCR residues are present is each CDR and outline a large binding footprint that suggests that the TCR binds to a protein (26). However, efforts to find an MHC or MHC-related presenting element failed (27, 28).

The discovery that mAbs specific for the butyrophilin (BTN) 3 extracellular domains can either block stimulation by IPP or zoledronic acid (the 103.2 mAb) or can induce stimulation of Vγ2Vδ2 T cells when bound to BTN3A1 (the 20.1 mAb) (29–31) identified BTN3A1 as a candidate protein in the stimulation process. siRNA or shRNA inhibition of BTN3A1 inhibited stimulation by HMBPP, IPP, and zoledronic acid (29, 30) and stimulation by human-mouse or human-hamster hybrid cell lines required the *p* arm of human chromosome 6 where the BTN3 genes are located (32, 33).

BTN3A1 is an Ig superfamily member with IgV and IgC domains and an intracellular B30.2 domain. Although one study proposed that BTN3A1 acted as a presenting element for prenyl pyrophosphates through a binding site on the IgV domain (32), our modeling of the B30.2 domain identified a potential basic binding site on the domain face that binds ligands in other B30.2-containing proteins (30). Subsequent crystallization of the BTN3A1 B30.2 domain confirmed the existence of the basic site and showed that an HMBPP analog could bind to the site in crystals (34) and HMBPP, IPP, and other analogs could bind to the B30.2 domain in solution (34–36). We tested BTN3A1 proteins with mutations in the proposed IgV site or the B30.2 site and showed that mutations in the B30.2 site abolished stimulation of Vγ2Vδ2 T cells in response to prenyl pyrophosphates (37). Taken together, these results outline a new paradigm for Ag recognition by T cells in which T cells monitor intracellular metabolism at the cell surface through intracellular sensing. However, the molecular basis that allows BTN3A1 to transmit signals to the extracellular surface for this monitoring is unclear.

Besides the B30.2 domain, the intracellular tail of BTN3A1 includes a 69 aa juxtamembrane segment spanning from the cell membrane to the B30.2 domain. This region is critical for the sensing function of BTN3A1 (36, 38). Whereas substitution of the transmembrane region from either BTN1A1 or fibroblast growth factor receptor 3 for the BTN3A1 transmembrane region does not affect sensing by BTN3A1, substituting juxtamembrane segments from other BTN and BTN-like (BTNL) proteins (e.g. BTN1A1, BTN2A1, BTN2A2, BTNL3, BTNL9, and ERMAP) completely abrogates sensing despite similar levels of surface expression compared with unmutated BTN3A1 (38). Moreover, mutation of BTN3A1 proteins with deletion of exon 5 or the dileucine motif in exon 5 in the juxtamembrane segment also completely abrogates sensing of either exogenous HMBPP or IPP in zoledronic acid-treated HeLa cells (36). Binding of HMBPP to the intracellular tail of BTN3A1 changes the conformation of the juxtamembrane region when analyzed by nuclear magnetic resonance (35) and small-angle x-ray scattering (39). The juxtamembrane region also mediates interactions with BTN3A2 and BTN3A3 proteins that are required for maximal stimulation of Vγ2Vδ2 T cells and high surface expression of BTN3A1 (40).

Despite this evidence for the importance of the juxtamembrane segment, extensive mutagenesis in this region does not affect or only partially diminishes sensing by BTN3A1. In one study, wild-type residues in the juxtamembrane region were substituted with AAGAA (in most cases) at 14 sites. Twelve of the mutant BTN3A1 proteins sense IPP accumulation after zoledronic acid treatment similarly to wild-type BTN3A1 (38). Mutation of other residues (S266AT267A and T274A) partially reduces stimulation by K562 cells with POM_2-C-HMBPP or zoledronic acid treatment (39). Also, mutation of four arginine residues

(residues 283, 285, 292, and 295) near the B30.2 domain to either alanine or lysine had no effect on the stimulation of Vγ2Vδ2 T cells by IPP accumulation due to zoledronic acid treatment as long as wild-type BTN3A2 was also present (40). Only mutation of residues immediately adjacent to the B30.2 domain (residues 299–305 and 306–310) completely abolishes stimulation of Vγ2Vδ2 T cells by IPP accumulation to zoledronic acid treatment (38). Thus, although the juxtamembrane segment is required, few essential residues can be identified.

In an earlier report, we proposed that a segment of the BTN3A1 juxtamembrane region interacts to form a coiled-coil dimer (37). Polypeptide chains can assume α-helical secondary structures through the formation of hydrogen bonds between backbone amide (N-H) donors to carbonyl (C=O) acceptors three to four residues apart. When two α helices supercoil, they form a rod-like tertiary structure, termed a coiled-coil dimer, that is stabilized by side chains along a core of seven ("a-g") residues (two turns of the α helix) (41). The side chains ("knobs") of the first ("a" position) and fourth ("d" position) residues are usually hydrophobic and termed "anchor residues" (42, 43). These anchor residues clearly favor aliphatic/methionine amino acids (63.9% at "a" and 70.4% at "d") but, surprisingly, polar amino acids (8.1% at "a" and 9.8% at "d") and charged amino acids (13.9% at "a" and 9.4% at "d") can also be present in these positions (44). The side chains pack into cavities (holes) surrounded by four side chains in the opposing α helix termed "knobs-into-holes" to stabilize the coiled-coil structure. The other residues face the outside of the rod and are predominantly polar or charged (41). Few glycines are present at any position (between 2–5%) and the few aromatic amino acids that are present are mainly tyrosines present at <5% at "a" and "d" positions. Certain amino acids, such as proline and cysteine, are almost never present. Although coiled-coil proteins can form complex oligomers, simple dimers are the most common.

Coiled-coil domains in proteins perform a variety of organizational and regulatory functions in cells acting as structural or interacting components (or both) (41, 45–48). Shorter coiled-coil domains (<6–10 heptad repeats [42–100 aa]) function as homo- and heterodimerization domains (45). For example, coiled-coil domains termed leucine zippers in the AP-1 transcription factor function as interaction domains for the c-Fos and c-Jun subunits (49, 50). Short coiled-coil domains in myotonic dystrophy protein kinase function to multimerize its subunits (51). Long domains of several hundred amino acids function as rods in intermediate-filament proteins of the cytoskeleton, tethers for Golgi organization and kinetochores, stalks for myosin, kinesin, and dynein motors, or as scaffolds for membrane structures (45) or for intracellular tripartide motif containing (TRIM) proteins (52). Both long and short coiled-coil domains can also function as spacers as evidenced by their length conservation in evolution independent of primary amino acid sequence variation (53).

In this report, we present evidence that two regions of the juxtamembrane segment of BTN3A1 form coiled-coil dimers. The first region starts at the plasma membrane and extends ~41 residues towards the B30.2 domain. Mutation of anchor residues predicted to disrupt this coiled-coil structure partially decrease or abrogate stimulation of Vγ2Vδ2 T cells by HMBPP. A second region (exon 8) dimerizes BTN3A1 B30.2 domains (34, 36). A critical tryptophan residue is identified in this region that when mutated to glycine is

predicted to destabilize the dimer when analyzed by molecular dynamics simulations. This exon and the tryptophan residue are conserved in almost all BTN and BTNL proteins with B30.2 domains, even in frogs and chickens. Other BTN and BTNL proteins are also predicted to have parallel coiled-coil dimers like BTN3 proteins. We propose that coiled-coil dimers likely space B30.2 dimers away from the plasma membrane and interact with other proteins.

Materials and Methods

Mutagenesis of BTN3A1 cDNA

The pCMV6-Entry expression plasmid for BTN3A1 (transcript variant 1, True ORF Gold) with myc and FLAG (DDK) tags on its C terminus was purchased from OriGene Technologies (Rockville, MD). Mutations in the membrane proximal coiled-coil domain of BTN3A1 were selected on the basis of our model of the coiled-coil dimer (37) and the prediction of anchor residues. The primers used to generate mutations in the BTN3A1 cDNA were designed using the Primer Design program (http://www.genomics.agilent.com/primerDesignProgram.jsp; Agilent Technologies, Santa Clara, CA) and synthesized by Integrated DNA Technologies (Coralville, IA). The length of the primers ranged from 30 to 40 nucleotides for a single mutation and from 50 to 60 nucleotides for a double mutation. The mutations in BTN3A1 were created by PCR using the primers and the QuikChange II Site-Directed Mutagenesis kit (Agilent Technologies). Expression plasmids containing mutated BTN3A1 cDNAs were purified using the QIAprep Spin Miniprep kit (QIAGEN, Valencia, CA) and the coding regions of the cDNAs were sequenced to confirm the presence of the mutations and to ensure that no other mutations were introduced.

Transfection of siRNAs and cDNAs

Silencer-27 siRNAs for BTN3A1 and control duplexes were purchased from OriGene and resuspended in the provided duplex buffer to obtain a 20 μM stock solution. The stock solution was further diluted to 5 μM with the same buffer for transfection or cotransfection with cDNA. For transfections, HeLa cells were plated at 1.7×10^5 cells/well in six-well plates 1 d prior to transfection. To transfect a well of HeLa cells with siRNA, 4 μl of a control siRNA or BTN3A1 siRNA oligo A was added to 100 μl of Opti-MEM I medium (Life Technologies, Grand Island, NY) and then mixed by vortexing. To transfect with cDNA, 150 ng of a control plasmid or the BTN3A1 expression plasmid was added to 100 μl of Opti-MEM I medium and then mixed by flicking. For cotransfection of BTN3A1 siRNA oligo A and BTN3A1 cDNA, 150 ng of cDNA was added to 100 μl of Opti-MEM I medium followed by 4 μl of siRNA and mixing. Then, 4.5 μl of the Attractene transfection reagent (Qiagen) was added to the siRNA and/or cDNA preparation, vortexed for 5 s, incubated at room temperature for 15 min, and added dropwise to a well of HeLa cells. Media was replaced at 24 and 48 h. After 72 h, the transfectants were trypsinized and harvested for analysis by flow cytometry and for use in T cell assays. Note that the BTN3A1 siRNA oligo A is specific for a sequence in the 3’ untranslated region of BTN3A1 that is not present in the BTN3A1 cDNA expression plasmid. Therefore, siRNA treatment only suppresses endogenous BTN3A1 mRNA.

mAbs and flow cytometry

To assess BTN3 surface expression, cells were stained with PE-conjugated anti-BTN3/CD277 (20.1, also termed BT3.1) (BioLegend, San Diego, CA) or with an isotype control PE-P3 mAb (eBioscience, San Diego, CA) on ice for 2 h. To assess BTN3 intracellular expression, cells were first fixed with fixation buffer on ice for 10 min and then permeabilized with permeabilization buffer (both buffers from Invitrogen, Carlsbad, CA) and stained on ice for 30 min with PE-20.1 mAb or PE anti-FLAG (DYKDDDDK) mAb (clone L5 from Biolegend), or an isotype control PE-P3 mAb diluted in permeabilization buffer. Flow cytometry analysis was done using the Becton Dickinson LSR II at flow cytometry facility of University of Iowa College of Medicine. Live cells were distinguished from dead cells using the LIVE/DEAD Fixable Dead Cell Stain kit (Invitrogen), and the data were plotted using FlowJo (Ashland, OR). Note that only the exogenous BTN3A1 proteins had FLAG tags on their C terminus.

T cell proliferation and cytokine secretion assays

The Vγ2Vδ2 CD8αα$^+$ 12G12 T cell clone was maintained by periodic restimulation with PHA. T cell-proliferation assays were performed as described previously (30). Assays for prenyl pyrophosphate (HMBPP) and PHA stimulation were done in singlet or duplicate using round-bottom 96-well plates using 0.5–1.0 × 10^5 12G12 T cells per well with 1.0 × 10^5 mitomycin C-treated HeLa APCs per well. Stimulating compounds were tested at one-half log dilutions, as indicated in the figure legends. Because there were differences in the maximal proliferation of Vγ2Vδ2 T cells stimulated by different HeLa transfectants, the data were normalized by setting the plateau proliferation values for HMBPP as 100% or, in cases where HMBPP proliferation did not reach plateau levels, using the HMBPP plateau values for control siRNA treated cells. To assess TNF-α responses, culture supernatants were harvested after 16 h and assayed for TNF-α levels by DuoSet sandwich ELISA (R&D Systems, Minneapolis, MN).

Human BTN3A1 structures and α helix, coiled-coil, and transmembrane predictions

BTN3A1 structures presented in this article were the BTN3A1 extracellular domains (Protein Data Bank [PDB] 4F80) (31), the BTN3A1 B30.2 domain with (PDB 4N7U) and without (PDB 4N7I) (*E*)-1-hydroxy-2-methyl-pent-2-enyl pyrophosphonate (HMBcPP) (34), the BTN3A1 B30.2 dimer (PDB 4V1P) (36), and the alternate BTN3A1 B30.2 dimer (PDB 5HM7). Residue numbering starts with residue 31, as used by Sandstrom (34) except when the full-length sequence including the signal peptide is being analyzed. To directly compare with other BTN3A1 extracellular domain structures, subtract one from the numbering used by Palakodeti (31), subtract three from the numbering used by Vavassori (32), or add 30 for the full length sequence.

Coiled-coil predictions were made using the MARCOIL v1.0 program (54) (http://bcf.isb-sib.ch/webmarcoil/webmarcoilC1.html) with the 9FAM coiled-coil emission matrix and the H HMM transition matrix settings by inputting the entire coding sequence of the longest isoform of the various BTN/BTNL family members. For BTN3 proteins, residues constituting the heptad register with the highest probability of forming a coiled coil were identified and plotted. The coiled-coil dimer of BTN3A1 is predicted to be from residue 242

to 282 (coiled-coil structure p >18%). Note that two heptad registers are predicted for alpaca (*Vicugna vicugna*) BTN3A3 with one starting with Q243 as a “d” residue with ~40% probability and the second starting with L242 as an “a” residue with ~58% probability. The Q243 heptad register is shown in the figures as it corresponds to the heptad register used by human BTN3A2/BTN3A3 and by bottlenose dolphin (*Tursiops truncatus*) BTN3A3. Summed coiled-coil probabilities (in which the probabilities for each of the possible registers for heptad repeats are added together) are also shown for BTN3 proteins and other BTN and BTNL molecules. Coiled-coil predictions for BTN3 proteins were also made using CCHMM (http://gpcr.biocomp.unibo.it/cgi/predictors/cc/pred_cchmm.cgi) (55), CCHMM_PROF (http://gpcr.biocomp.unibo.it/cgi/predictors/cchmmprof/pred_cchmmprof.cgi) (56), and MultiCoil2 (http://cb.csail.mit.edu/cb/multicoil2/cgi-bin/multicoil2.cgi) (57) programs as well as one variant of the COILS program (COILS v2.1 (https://npsa-prabi.ibcp.fr/cgi-bin/npsa_automat.pl?page=npsa_lupas.html). Transmembrane predictions were made using the TMHMM v2.0 program (http://www.cbs.dtu.dk/services/TMHMM/). α helix predictions were made using the JPred4 program (http://www.compbio.dundee.ac.uk/jpred4/index.html) (58).

Models of the predicted coiled-coil dimer were made using the CCBuilder2 program (59) (http://coiledcoils.chm.bris.ac.uk/ccbuilder2/builder). Models were made using standard settings assuming a parallel homodimeric structure using residues 243–282 (273–312 for full length) for human BTN3A1, BTN3A2, and BTN3A3 and alpaca and dolphin BTN3A3. BTN3A1 was modeled with residue 243 at the “c” position of the heptad repeat whereas all other BTN3 proteins were modeled with residue 243 at the “d” position. A second model of BTN3A1 termed “BTN3A1-Alternative Register” was also modeled with residue 243 at the “d” position. Models of human BTN3 proteins were further refined using the “Optimize” function of the CCBuilder2 website.

Homology modeling of BTN and BTNL B30.2 homodimers was done using MODELLER (PyMOD plugin version 2.0) (60, 61) and PyMOL X11 version 1.8.6.2. B30.2 dimer models were based on the BTN3A1 B30.2 structure (PDB 4V1P) and the modeled B30.2 sequences aligned using ClustalW with optimization level set to high and additional energy minimization selected.

The BTN3A1 structural model is composed of the crystal structure of the BTN3A1 extracellular homodimer (PDB 4F80) and a model of the region encoded from the extracellular domains through the juxtamembrane domain (exons 4–5) as a coiled-coil dimer using CCBuilder2, and the α helix region (exon 5–7) from the BTN3A1 B30.2 structure (PDB 5HM7). The extended model uses the BTN3A1 B30.2 dimer with the higher resolution 4N7I B30.2 monomer aligned to the 4V1P B30.2 dimer. The compact model uses the alternative BTN3A1 B30.2 structure (PDB 5HM7) where dimerization is not through the dimerization exon and where the α helix region (exon 5–7) is aligned with the end of the coiled-coil model. Note that this results in steric clash such that this structure would require a less acute angle at the B30.2 domain.

All figures were produced using PyMOL X11 version 1.8.6.2 (Schrödinger, LLC, New York City, NY). The BTN3A1 domains are identically scaled using a PyMOL script. Electrostatic

surface potential was calculated by the APBS 2.1 PyMOL plugin (62) with PyMOL-generated PQR files, hydrogens, and termini for the extracellular domains and with either internally generated PQR files or, if required, externally generated PQR files from the PDB2PQR website (http://nbcr-222.ucsd.edu/pdb2pqr_1.8/) using the PARSE forcefield for the B30.2 domain, and PyMOL generated PQR files, hydrogens, and termini for coiled-coil dimers. Surface potentials are colored from red (negative potential, −10 kT) to blue (positive potential, +10 kT).

Alignments were done by the Clustal W method in MegAlign v15.0.0 (Lasergene, DNAStar, Madison, WI). Exon boundaries for BTN and BTNL proteins were from the Consensus CDS database at the National Center for Biotechnology Information website when available, or determined from genomic and mRNA sequence data. Sequences for the coiled-coil exon and the dimerization exon are from the frog (*Xenopus tropicalis*) BTN1A1-homolog, XP_012823386.1, and from the red jungle fowl (chicken; *Gallus gallus*) BTN1A1-homolog (also termed Tvc), NP_001029989.

Molecular dynamics simulations of BTN3A1 B30.2 dimers

To assess the effects of mutations in the dimerization domain of BTN3A1, models of 14 mutant BTN3A1 B30.2 homodimers were made using the crystal structure of human BTN3A1 B30.2 dimers, residues 295–513 (PDB 4V1P) (36). Mutants were modeled by reconstructing side chains of mutated residues using MODELLER version 2.1 (60, 61). All models were constructed as dimers. The AMBER99SB-ILDN (63–65) force field was used to construct the model. Models were then solvated in 150 mmol L^{-1} NaCl solution, with a solvation thickness of 15 Å. Each model comprised ~134,000 atoms. For each mutant (or wild-type protein), four independent equilibration and simulation runs were performed. The model was first equilibrated with a 1-ns NPT run with all heavy atoms restrained to the initial structure. The harmonic restraint potentials were used with the spring constants of 2.39 kcal mol^{-1} $Å^{-2}$ (1.0×10^3 kJ mol^{-1} nm^{-2}). Then, molecular dynamics simulations with NPT conditions (300 Kelvin, 1.013 bar) were assessed for an 80-ns period without the restraint potential. Two sets of four replicate simulations were performed for each starting structure with different initial velocities at the beginning of the equilibration. The averages and standard deviations of the root-mean-square (RMS) deviation were calculated using the 4V1P structure as a reference either for all the Cα atoms in the structure or for the Cα atoms of the helices of the B30.2 dimer. Although higher values were noted for the RMS deviation for all of the Cα atoms, the RMS deviation for the Cα atoms of the helices correlated better with the reported biological activity of mutant BTN3A1 proteins. Therefore, the RMS deviations for the Cα atoms of the helices of the B30.2 dimer are shown in the figures.

Results

Juxtamembrane segments of BTN3 proteins are predicted to assume α helices that interact to form coiled-coil dimers

Although the juxtamembrane segment of BTN3A1 plays a vital role in its function in activating Vγ2Vδ2 T cells, the molecular basis for this role is unclear. We therefore sought to predict its structure. When the sequence of the BTN3A1 juxtamembrane region is

evaluated by the JPred4 program, this region is predicted to assume an α helix secondary structure starting immediately after the transmembrane segment and extending to glycine 293 and then resuming at aspartic acid 301 and ending four amino acids before the B30.2 domain at leucine 306. The α helix prediction is consistent with a recent crystal structure encompassing part of the juxtamembrane region with the B30.2 domain from BTN3A1. In the 5HM7 structure, the juxtamembrane region assumes an α helix with a gap/bend (66). However, the α helix gap is shorter than predicted spanning only arginine 292 to aspartic acid 294. This gap in the α helix is predicted for all BTN3 proteins with the conservation of arginine 292 to aspartic acid 294 in five out of six proteins. Thus, the BTN3A1 juxtamembrane region is predicted to assume an α helix starting at the transmembrane and extending to the B30.2 domain with crystal evidence for the distal portion of this α helix and for the gap between residues 292 to 294. BTN3A3 and BTN3A2 are also predicted to assume α helices starting immediately after their transmembrane segments as are BTN3A3 homologs from alpacas (*Vicugna pacos*) and bottlenose dolphins (*Tursiops truncatus*) (as indicated by the red lines under the BTN3 sequences in Fig. 1A). As reported by the Herrmann laboratory, alpacas and dolphins have single functional BTN3A3 homologs in their genomes along with Vγ2 and Vδ2 V genes that would allow their γδ T cells to respond to isoprenoid metabolites sensed by their BTN3A3 homologs (67, 68).

The extracellular domains of BTN3A1 form a “V” shaped dimer through IgC-IgC interactions (31, 66) suggesting that the intracellular domains might also dimerize. As discussed above, α helices can interact to form coiled-coil dimers where amino acid side chains protrude into an adjacent α helix to stabilize the structure. The interacting amino acids are regularly spaced and constitute the “a” and “d” positions in a heptad motif. To determine if coiled-coil segments are predicted for BTN3A1, its sequence was evaluated by five programs that predict coiled-coil structures: MARCOIL (54), Multicoil2 (57), CCHMM (55), CCHMM_PROF (56), and COILS v2.1 (44). All five programs predict the presence of coiled-coil dimers in the juxtamembrane segment of BTN3A1 and the other BTN3 proteins (Fig. 1B and Supplemental Fig. 1). The MARCOIL program predicts a coiled-coil dimer starting at the cell membrane and extending to leucine 282 for BTN3A1 (Fig. 1B, left panel). Similar coiled-coil dimers are predicted for human BTN3A2 and BTN3A3 (Fig. 1B, middle and right panels). BTN3A3 homologs from alpacas and dolphins are also predicted to have coiled-coil dimers with the coiled-coil dimer of the dolphin BTN3A3 homolog predicted with very high confidence (>97% probability) in a single heptad register. The register of the heptad repeats for human BTN3A2 and BTN3A3 is identical to that used by alpaca and dolphin BTN3A3-homologs but differs from that predicted for BTN3A1 (Fig. 1A, residues shaded green are predicted to be “a” or “d” anchor residues). This is consistent with the fact that the human BTN3A3 juxtamembrane region shares 66.7% homology with the BTN3A2h juxtamembrane region whereas BTN3A1h shares only 34.9% (BTN3A2h) and 55.1% (BTN3A3h) homology. The Multicoil2 program similarly predicts coiled-coil dimers in a single heptad register, with BTN3A1h, BTN3A2h, BTN3A3a, and BTN3A3d proteins each predicted to contain a coiled-coil dimer with probabilities between 80 and 100% (Supplemental Fig. 1B). However, the predicted register for the heptad repeats for human BTN3A1 corresponds to that noted by the MARCOIL and Multicoil2 programs for the other BTN3 proteins.

The MARCOIL program predicts coiled-coil dimers of similar length for all of the BTN3 proteins. However, the lengths predicted by other programs vary (Supplemental Fig. 1A shows the predicted location of the coiled-coil dimers by the different programs). The coiled-coil dimers were all predicted to start slightly after the transmembrane segment and to generally end between residues 312 and 320. However, the CCHMM, CCHMM_PROF, and Multicoil2 programs generally predicted longer coiled-coil-dimers particularly if the full-length sequences were analyzed by the CCHMM and CCHMM_PROF programs.

Models of the coiled-coil dimers based on the MARCOIL predictions (Fig. 1C) show that they differ in their surface potential with the membrane proximal regions of BTN3A1 predicted to be basic whereas the other coiled-coil dimers are less so. Thus, the juxtamembrane regions of BTN3 proteins from humans and other mammals are predicted to assume α helices that interact to form parallel coiled-coil dimers of similar length that start at the cell membrane and end 15–30 aa prior to the B30.2 domain.

Mutation of anchor residues in the predicted coiled-coil dimer of BTN3A1 reduces or abrogates prenyl pyrophosphate stimulation of Vγ2Vδ2 T cells

The stability of coiled-coil dimers is dependent on the side chains of amino acids at the “a” and “d” positions in the heptad repeat and the presence of polar or charged residues at the other positions. The side chains (knobs) of “a” and “d” amino acids on one helix pack into a space (hole) surrounded by 4-aa side chains of the facing helix. Glycines lack side chains and destabilize coiled-coil dimers especially if substituted for amino acids at the “a” or “d” positions in the heptad motif. Moreover, although the yeast GCN4 leucine zipper transcription factor tolerates single amino acid substitutions at “a” and “d” amino acids, tandem mutations of “a” amino acids generally abolished activity (69). Thus, to assess the importance of the predicted coiled-coil dimers of BTN3A1, adjacent “a” and “d” anchor residues were mutated to glycine at five positions that were proximal, medial, or distal to the transmembrane segment (Fig. 2A). The effect of these mutations was then assessed by transfection of mutant or wild-type BTN3A1 cDNA into HeLa cells treated with siRNA specific for endogenous BTN3A1 as done previously (30, 37). Transfected HeLa cells were then analyzed by flow cytometry for their surface and intracellular expression of BTN3A1 and for their ability to stimulate Vγ2Vδ2 T cells to proliferate and release TNF-α in response to HMBPP or the PHA mitogen.

Transfection of BTN3A1 cDNAs with glycine substitutions increased intracellular BTN3A1 levels compared with wild-type BTN3A1 cDNA. When assessed by anti-FLAG mAb, wild-type BTN3A1 was expressed at a mean fluorescence intensity (MFI) of 455 whereas the five glycine mutants were expressed at MFIs between 810 and 1278 (Fig. 2B, third panels from left). There were corresponding minor decreases in the surface expression of BTN3 (all <2-fold) with an MFI of 1159 for wild-type BTN3A1 versus 610–1117 for the glycine mutants) (Fig. 2B, left panels). The results suggest that there may be increased intracellular retention of the mutant BTN3A1 proteins, perhaps due to decreased dimerization, misfolding, or reduced association with BTN3A2 or BTN3A3 proteins (40). However, the magnitude of the retention varied between experiments and thus additional studies will be needed to confirm this finding.

Glycine mutations in BTN3A1 decreased or abrogated the stimulation of proliferation and TNF-α release by Vγ2Vδ2 T cells in response to HMBPP. Mutation of anchor residues to glycine in the middle of the coiled-coil dimer (E262G W265G and W265G K269G) abrogated stimulation of Vγ2Vδ2 T cells by HMBPP with both proliferation and TNF-α release at baseline levels (EC_{50} increased by >50-fold) but had no effect on stimulation by the PHA mitogen (Fig. 2B, right four panels). Mutations of anchor residues close to or distant from the membrane also decreased the potency of HMBPP stimulation by 6-fold for the membrane proximal mutations (EC_{50} = 1.2 nM for K248G F251G) whereas distal mutations decreased by 12.5-fold (EC_{50} = 2.5 nM) for Q272G V276G and 5-fold (EC_{50} = 1.0 nM) for V276G L279G. The potency of HMBPP stimulation for TNF-α secretion was reduced by similar levels for the five mutant proteins (Fig. 2B, right panels).

The effect of mutations in the BTN3A1 juxtamembrane region on the stimulation of Vγ2Vδ2 T cells has been also extensively studied by the Scotet laboratory with 62 mutations located at fourteen sites (38). For most of their mutant BTN3A1 proteins, five contiguous residues at a site were replaced with AAGAA. Five of their mutant BTN3A1 proteins had alanine mutations in the same residues where glycine mutations were made in this study (Fig. 3A). For example, the mut05 BTN3A1 protein had alanine mutations at the predicted anchor residues, aspartic acid 262 and tryptophan 265, instead of the glycine mutations made in this study.

Although glycines may destabilize α helices because of their lack of side chains and high conformational flexibility, this is dependent on their relative position in the helix and on the surrounding amino acids (70, 71). The BTN3A1 mutations reported in this study and in the Scotet study did not alter the prediction that the juxtamembrane region assumes an α helix (represented by the red line under the sequences in Fig. 3A). However, differences were noted in coiled-coil dimer predictions. Unlike unmutated BTN3A1, BTN3A1 proteins with glycine mutations at anchor residues were not predicted to have a coiled-coil dimer (Fig. 3B), In contrast, four out of five BTN3A1 mutant proteins from the Scotet study, were still predicted to assume a coiled-coil dimer. This is consistent with studies on other proteins with a coiled-coil dimer where substitution of alanine (with its short hydrophobic side chain) at anchor residues only moderately affects coiled-coil stability whereas glycine substitutions have severe effects (42, 43, 51). Importantly, the corresponding alanine mutations at anchor residues in BTN3A1 did not significantly affect stimulation of Vγ2Vδ2 T cells by the aminobisphosphonate, zoledronic acid (which is functionally equivalent to using HMBPP) (mutant protein activities summarized in Fig. 3C). In fact, none of the BTN3A1 proteins with mutations in the proximal juxtamembrane region exhibited significant decreases in their ability to stimulate Vγ2Vδ2 T cells despite mutating 51 residues at twelve sites (38). Taken together, these findings suggest that the juxtamembrane regions of BTN3A1 assume α helices that interact to form a critical parallel coiled-coil dimer with a gap in the α helices near the B30.2 domain.

Coiled-coil dimerization interface of BTN3A1 B30.2 domains is critical for the sensing of prenyl pyrophosphates

The distal α-helical segment of the juxtamembrane region of BTN3A1 (Fig. 1A) forms a second short coiled-coil dimer that dimerizes the B30.2 domains of BTN3A1 in crystal structures (34, 36). Close up views show the positioning of tryptophan 302 (“d” residue) at the center of the B30.2 dimer interface (Fig. 4). The importance of this region of BTN3A1 in the sensing of prenyl pyrophosphates is supported by the fact that mutations in this region abrogate stimulation of Vγ2Vδ2 T cells by zoledronic acid (38, 40). One mutant (mut13) overlaps the area where the tryptophan at residue 302 lies and a second (mut14) mutates residues in the distal portion of the dimer interface (detailed in Fig. 5A). Models of the interface for the two mutant BTN3A1 proteins as well as other potential mutant proteins are shown in Fig. 5B.

To assess the effect of these and other amino acid substitutions in the coiled-coil dimer interface region, molecular dynamics simulations of BTN3A1 dimer stability were performed and the RMS deviation was measured relative to the 4V1P B30.2 wild-type or mutant dimer starting structure either for all the Cα atoms or for the Cα atoms of the helices of the B30.2 dimer. An earlier study reported that the 4N7I BTN3A1 B30.2 dimer (residues 298–483) quickly dissociates (~100 ns) (66). To determine the stability of the longer 4V1P BTN3A1 B30.2 dimer (residues 295–483) used in this study, molecular dynamics simulations were performed until an accumulated trajectory time of 400 ns was reached. This was repeated 4 times. The 4V1P BTN3A1 B30.2 dimer was stable in all the replicates and showed no evidence for dissociation (data not shown). In contrast, molecular dynamics simulations performed using a truncated B30.2 dimer (residues 298–483) corresponding to that used by Gu et al. (66), but based on the 4V1P structure, destabilized over ~80 ns with each of the 4 replicates showing pronounced RMS deviations (data not shown).

Given the stability of the wild-type B30.2 dimer, the stability of B30.2 dimers with mutations in the dimerization region were next assessed using models based on the 4V1P structure and measuring the RMS deviation relative to the 4V1P B30.2 wild-type or mutant dimer starting structure for the Cα atoms of the helices of the B30.2 dimer. B30.2 dimers with mutation of tryptophan 302 to glycine showed poor stability of the dimer interface over an 80-ns simulation (Fig. 6A). In contrast, B30.2 dimers with single glycine mutations in residues 301, 303, 304, 307, 308, 309, and 310 were stable, consistent with a critical role for tryptophan 302 in determining dimer stability. Molecular dynamics simulations of dual glycine mutants underscore the importance of tryptophan 302 because only mutant B30.2 dimers with a tryptophan 302 to glycine mutation were unstable (Fig. 6B). B30.2 dimers with mutations to other aromatic amino acids (Y299W W302Y) or to glycines at leucine 306 and phenylalanine 307 were stable. Finally, the mut13 BTN3A1 B30.2 dimer, where tryptophan 302 is mutated to alanine and other adjacent residues to either alanine or glycine, was also unstable (Fig. 6C). Although mut14 was not as destabilizing as mut13, this mutation did destabilize the dimer to a moderate degree and also introduced an alanine at proline 309. Proline residues introduce kinks in α helices, so this mutation likely alters the orientation of the helix to the B30.2 domain. Both mut13 and mut14 mutations completely abrogate zoledronic acid stimulation of Vγ2Vδ2 T cells (38). Qualitatively similar results

were noted in a second series of molecular dynamics simulations (4 replicates each, 80 ns) in which the RMS deviation for all the Cα atoms was measured relative to the 4V1P B30.2 wild-type or mutant dimer starting structure (data not shown). Therefore, molecular dynamics simulations of mutant BTN3A1 proteins point to a critical role for tryptophan 302 in stabilizing the B30.2 dimer. Moreover, mutation of the residues surrounding the tryptophan (changing Glu-Trp-Lys to Asp-Trp-Arg) did not affect stimulation whereas loss of the tryptophan (changing Glu-Trp-Lys to Asn-Lys-Ser) abolished stimulation (40). The loss of BTN3A1 function with mutation of tryptophan 302 and adjacent residues suggests that dimerization of B30.2 domains is required for the function of BTN3A1.

Juxtamembrane regions of human and murine BTN and BTNL family proteins have conserved exons for coiled coil and B30.2 dimerization and are predicted to assume α helices that, for longer regions, may associate to form parallel coiled-coil dimers

BTN and BTNL proteins are evolutionarily conserved and can be found in fish, amphibians, reptiles, birds, and mammals. To determine if the juxtamembrane regions of other human and mouse BTN and BTNL proteins show similarities to BTN3 proteins, their juxtamembrane sequences were analyzed along with the BTN3A3 homologs from alpacas and dolphins (Fig. 7). The transmembrane regions were predicted for each protein and varied in length from 20 to 28 aa in length (shaded blue in Fig. 7A). The juxtamembrane regions are encoded on between one and seven exons, with those with B30.2 domains having between three and seven exons, except for BTNL10m that has one exon (exon boundaries are delineated by amino acids in red, Fig. 7A). Like BTN3 proteins, all BTN and BTNL proteins with B30.2 domains (except for BTNL10m) were predicted to have juxtamembrane regions that assume α helices (predicted α-helical regions are underlined with red lines, Fig. 7A). The juxtamembrane regions of human and murine BTN and BTNL proteins have zero (six proteins), one (seven proteins), or two (four proteins) predicted gaps in their α helices that could allow for bending of the helix. There is only one BTN/BTNL protein, BTN1A1h, with a proline residue in its juxtamembrane region, although the gap in its α helices does not include the proline residue.

One juxtamembrane exon is conserved between most BTN and BTNL proteins, whether or not they contain B30.2 domains, including those from birds (chickens [*Gallus gallus*]) and amphibians (frogs [*Xenopus tropicalis*]) (Fig. 7B). Only BTNL2 proteins that have minimal juxtamembrane segments with no B30.2 domains and the BTNL10 proteins (which may be a pseudogene in humans and may not be expressed in mice) lack this exon. The exon has seven residues (nine if boundary residues are included) with the leucines at positions 2 and 6 being highly conserved. BTN1A1 and MOG proteins have conservative replacements at position 2, and only BTNL4m has a basic residue at position 6. There is also a leucine or a glutamine at position 3 for 14 out of 19 proteins. The spacing of the leucine/glutamine residues allows them to potentially function as “d” (position 2) and “a” (position 6) or as “a” (position 3) and “d” (position 6) anchor residues for a coiled-coil dimer (Fig. 7B). This could allow the dimerization of this region.

The exon encoding the B30.2 dimerization domain of BTN3A1 is also conserved in all BTN/BTNL proteins with B30.2 domains (except for BTNL10m) (Fig. 7C). A tryptophan at

position 1 is conserved for all BTN/BTNL proteins, except for BTN1A1m. This is the residue that is predicted to be critically important in maintaining B30.2 dimerization in BTN3A1 in our molecular dynamics simulations (Fig. 6). A basic arginine or lysine residue at position 2 is also present in all of the BTN/BTNL proteins with B30.2 domains. Underscoring its importance, mutations in this region of BTN3A1 abrogate sensing of prenyl pyrophosphate (38). Moreover, frogs (class Amphibia) and chickens (class Aves) also conserve this region as a separate exon with similar sequences. The high conservation of this region in human and murine BTN/BTNL proteins (mammalian) as well as in amphibian and avian BTN proteins with B30.2 domains suggests that dimerization of B30.2 domains may occur in other BTN/BTNL proteins besides BTN3A1 and have similar important roles.

Given the conservation of the dimerization exons prior to B30.2 domains, models of B30.2 dimers for human and murine BTN and BTNL proteins were made based on the structure of the BTN3A1 B30.2 dimer (PDB 4V1P) (Fig. 8). Although the positioning of the binding sites is predicted to be similar to that of BTN3A1 (Fig. 8, left and middle panels for side views and top views), the conformation and surface potential of the biding sites can be very different, with surface potentials ranging from acidic to basic and from pockets (BTN3A1h and BTN3A3h) to more elongated sites (BTNL9h and BTNL9m) (Fig. 8, right panels). However, the characteristics of the binding sites are conserved between human and mouse orthologous proteins, such as BTNL9 and ERMAP.

The parallels between BTN3A1 proteins and other BTN and BTNL proteins suggest that other BTN/BTNL proteins might also be predicted to form coiled-coil dimers. When analyzed by the MARCOIL program, BTN2A1h, BTN2A2h/m, BTNL9h/m, and ERMAPh/m were all predicted to have coiled-coil dimers. Proteins such as ERMAPh/m and BTNL9h have a single predicted heptad register of >95% probability (Fig. 9). In contrast, proteins with short juxtamembrane regions, such as BTNL3h, BTNL8h, and BTN1A1h/m (juxtamembrane regions of 29, 30, and 34/34 residues, respectively), were predicted to assume α helices but not coiled-coil dimers (Figs. 7, 9 and Table I). However, there were also several BTNL proteins with long juxtamembrane domains without predicted coiled-coil dimers (BTNL1m [69 aa], BTNL4m [70 aa], and BTNL6m [68 aa]), suggesting that length was only one determinant of the presence of coiled-coil dimers (Table I) or that they might form heterodimers that cannot be predicted with present programs. Thus, the juxtamembrane regions of other BTN/BTNL proteins that have B30.2 domains show similarities to BTN3A1 in that most assume α helices with many longer regions predicted to form coiled-coil structures. They share an exon that could allow for dimerization of the intervening region and another exon for dimerization of the B30.2 domain. Our results suggest that an intracellular coiled-coil dimer stalk might serve to connect the extracellular domains of BTN3A1 to a B30.2 dimer (Fig. 10A, extended model). It is possible that the B30.2 domains alter their position relative to the coiled-coil stalk upon binding prenyl pyrophosphates (Fig. 10A, compact model). Based on the proposed structures, various models can be proposed for the molecular basis for BTN3A1 stimulation of Vγ2Vδ2 T cells (Fig. 10B).

Discussion

The intracellular juxtamembrane region of BTN3A1 is essential for its function, but the role it plays is unclear. In this study, we find that the juxtamembrane region is predicted to form an α helix that starts at the cell membrane and extends to the B30.2 domain, with one gap at residues 291–293. The presence of the α helix and the gap is confirmed by a crystal structure of the B30.2 domain (PDB 5HM7) that includes this gap and the distal portion of the α helix (66). Most of the α helix is predicted to homodimerize to form a parallel coiled-coil dimer that extends from the membrane to residue 281. Consistent with this prediction, glycine mutation of adjacent anchor residues in the coiled-coil dimer (that are essential for stabilizing the coiled-coil structure) either partially or completely abrogated the ability of BTN3A1 to support HMBPP-stimulation of Vγ2Vδ2 T cells. Although mutant BTN3A1 proteins were present on the cell surface at near-normal levels, there were higher intracellular levels, suggesting reduced transport to the surface, possibly due to disruption of protein interactions or protein misfolding.

A second short coiled-coil/dimerization region is found immediately before the B30.2 domains in BTN3A1 B30.2 dimers (34, 36). On molecular dynamics simulations, mutation of the tryptophan residue at position 302 to glycine either alone or in combination with other mutations destabilizes this dimer. Consistent with the simulation results, mutation of this residue and others in its immediate vicinity abrogates stimulation of Vγ2Vδ2 T cells (38). Moreover, this tryptophan residue is encoded on a short exon that is conserved in almost all BTN and BTNL proteins with B30.2 domains in mammals (humans and mice) as well as in chickens and frogs. These findings suggest that the B30.2 dimer structure is conserved for other human BTN and BTNL proteins as well as between species. A second conserved exon is predicted to be part of the coiled-coil dimers that are predicted in many but not all BTN and BTNL proteins. The conservation of these exons and predicted coiled-coil dimers suggests that the juxtamembrane regions have similar but not identical structure for many BTN and BTNL proteins with B30.2 domains.

The molecular dynamics simulation results reported in this study differ from those of the Adams laboratory, who reported that the BTN3A1 B30.2 dimer quickly dissociates (~100 ns) in molecular dynamic simulations with the CHARMM force field (66). In contrast, we observed no destabilization of the B30.2 dimer in four simulations of 400 ns (data not shown). A possible reason for this difference is that the Adams laboratory used a shorter B30.2 dimer (PDB 4N7I) starting from residue 298, whereas we used a longer B30.2 dimer (PDB 4V1P) starting from residue 295. In our simulations, we observed that hydrogen bonds formed between 451N:296O and 298N:449O. The deletion of residues 295–297 and the capping of N termini by NH_3^+ groups, as in the 4N7I dimer, results in the loss of these hydrogen bonds that likely explains the differences in stability. To confirm this, we performed simulations with a B30.2 dimer based on 4V1P in which residues 295–297 were deleted. Deletion of residues 295–297 tended to destabilize the B30.2 dimer in 80-ns simulations. Thus, in addition to exon 8 (spanning residues 301–310 of BTN3A1) that is conserved between BTN and BTNL proteins, additional residues from exon 7 (spanning residues 292–300) are required for efficient stabilization of the BTN3A1 B30.2 dimers.

Coiled-coil dimers in the juxtamembrane segment of BTN3A1 and the other BTN3 proteins are predicted by several programs. All of these programs are based on analyzing the sequences of proteins with and without coiled-coil domains identified in crystal structures (the learning set) to obtain amino acid probability distributions for each of the heptad positions of coiled-coil segments. Then algorithms are used to predict the presence of coiled-coil regions from the amino acid sequence of a protein. Coiled-coil prediction programs were recently tested with 1042 proteins with 2176 coiled-coil domains and 601 proteins without coiled-coil domains, as determined from their crystal structures (72). The most-accurate programs all use some form of hidden Markov model. The CCHMM_PROF program made 219 true predictions had no false-positive predictions for 100% precision (the CCHMM program was not tested). Multicoil2 is also very precise (precision was 99%) while MARCOIL-H is slightly less precise (precision was 95%). Thus, although many proteins with coiled-coil domains are not identified, when coiled-coil domains are predicted, these programs are correct with few or no false predictions. The study found that the CHHMM_PROF and the Multicoil2 programs were the most accurate for the detection of coiled-coil domains of both short and long lengths (72). In an earlier comparison, MARCOIL was felt to be superior to the COILS, PCOILS, PairCoil2, and MultiCoil programs and was especially good for proteins with short coiled-coil domains (73), like those predicted for BTN proteins. In light of these results, the fact that all of the programs predict coiled-coil dimers in the juxtamembrane region of BTN3 including human BTN3A1 and BTN3A3 proteins strongly supports their presence.

The existence of coiled-coil dimers in human BTN3 proteins is also supported by the fact that the alpaca and dolphin BTN3A3 proteins are highly homologous with human BTN3A1, sharing 71.0% and 71.4% sequence identity, respectively (Supplemental Figs. 2–4). In studies in which the structures of related proteins were compared, proteins sharing >50% sequence identity and without major insertions or deletions have common core structures that differ little from each other (<1 Å RMS deviation) (74). However, if the homology drops to <20%, then there can be large structural differences. Given the high homology of the BTN3 proteins (even the coiled-coil regions of BTN3A1 are 36.6% homologous to alpaca and dolphin), it is likely that human BTN3 proteins share key structural elements, including the coiled-coil dimers predicted with high certainty by all of the prediction programs for BTN3A3a and BTN3A3d.

We found that glycine mutations in anchor residues in the predicted coiled-coil dimer of BTN3A1 either diminished or nearly abolished stimulation of Vγ2Vδ2 T cells by prenyl pyrophosphates. In contrast, the Scotet laboratory reported that alanine mutations of many of the same residues did not significantly decrease zoledronic acid stimulation of Vγ2Vδ2 T cells (38). The difference in BTN3A1 function observed between glycine mutants and alanine mutants could be either because of their effects on coiled-coil stability or because they introduce gaps or kinks in the α helices that are required for coiled-coil structures. Glycines lack side chains that help stabilize both coiled-coil dimers and α helices. For coiled-coil structures, the lack of a side chain does not allow for the knob-in-hole interaction between the α helices to form the coiled-coil structure (41, 46, 75). Consistent with this fact, glycine mutations at anchor residues diminish coiled-coil structure probability much more than alanine mutations, such that the MARCOIL program no longer predict coiled coils in

BTN3A1 proteins with two glycine mutations, while still predicting these structures in most BTN3A1 proteins with alanine mutations (Fig. 3B).

Similar mutations have been used to study the role of the coiled-coil domain of myotonic dystrophy protein kinase (51). Glycine mutations in three anchor residues of the coiled-coil region of this protein impair its ability to homo- and heteromultimerize. The glycine mutations also partially diminish the activity of its kinase domain and abolish its localization to mitochondria (51). Their results and ours are consistent with a study that found that glycine mutation at a “d” anchor residue in the center of a typical coiled-coil segment results in the lowest coiled-coil stability out of the 19 aa (43) and the 16th-lowest stability out of 18 aa at an “a” residue (42). Moreover, glycines are rarely present at the “a” and “d” positions in coiled-coil dimers (42, 43).

In contrast to their effects on coiled-coil predictions, glycine mutations did not affect the predictions for α helices in the juxtamembrane region of BTN3A1 (Fig. 3B). Glycines confer less stability to α helices because their lack of side chains gives them high conformational flexibility, making them entropically expensive to adopt constrained α-helical structures (71, 76). However, the magnitude of this effect depends upon their position, as they are less destabilizing at the ends of coiled-coil domains (70, 77, 78), and lone glycine residues by themselves do not cause bends or gaps in α helices (79). Instead, glycines tend to be located at the hinge points of bends that are initiated by other upstream and downstream residues (79). Proline residues are the most common cause of bends in α helices (79). Consistent with straight α helices, the only prolines in the juxtamembrane regions of human and mouse BTN and BTNL proteins are one in BTN1A1h (with its very short juxtamembrane region) and one in the B30.2 dimerization domains of BTNL4m (Fig. 7A). There are prolines in BTN3A1h and BTN3A3h, but they are at the start of the B30.2 domain. Bends in α helices are also caused by upstream and downstream oppositely charged amino acids, serines/threonines, or aromatic amino acid motifs separated by 2–3 aa (79) and these are present at the few predicted gaps in the α helices of the juxtamembrane region of BTN and BTNL proteins (Fig. 7A). However, none of these motifs are present in the juxtamembrane region of BTN3A1, and the dual glycine mutations made do not create any new bend motifs because three glycines are required to create GxxGxxxG and GxxxGxxG bend motifs (79, 80). Therefore, based on our present understanding of the effects of glycine as detailed above, we interpret the loss of function by the glycine mutations to be due to their disruption of the coiled-coil structure rather than the α helices of BTN3A1.

Attempts to determine the structure of the juxtamembrane region by small-angle x-ray scattering found evidence for a relatively globular structure with nuclear magnetic resonance analysis predicting only a short α helix at the C-terminus (39). This study used the entire juxtamembrane region (68 aa) that had poor solubility rather than the predicted coiled-coil segment (N-terminal 40 aa) of human BTN3A1 molecule that might form a more-stable structure. Also, the transmembrane segment is omitted that might serve to help stabilize the membrane-proximal portion of the coiled-coil dimer. The crystal structure of the B30.2 domain and juxtamembrane region reveal that at least the C-terminal 34 aa residues of the region assume an α helix with a single gap (66), consistent with the prediction of the JPred4 program. It remains possible that a portion of the juxtamembrane coiled-coil dimer is

actually disordered, which would allow the region to assume a more-globular shape or to fold/bend more acutely than allowed by a relatively rigid coiled-coil dimer. Also, the coiled-coil dimer of dolphin BTN3A3 is predicted with high confidence (Fig. 1B) and therefore might be more stable and more amendable to structural analysis.

The high confidence prediction (>97% in one heptad register) for a coiled-coil dimer in the juxtamembrane region of the orthologous BTN3A3 protein from bottlenose dolphins provides further support for the presence of coiled-coil dimers in human BTN3A1, as discussed above. Given the strong homology between the amino acid sequence of dolphin BTN3A3 and other BTN3 proteins (69–86% amino acid identity, Supplemental Figs. 2–4), we feel that it is likely that the corresponding juxtamembrane regions of other BTN3 proteins also form coiled-coil structures. Moreover, many human and mouse BTN/BTNL proteins are predicted to have coiled-coil dimers (Figs. 7, 9). Proteins such as BTN2A1h, BTN2A2h/m, BTNL9h, and ERMAPh/m are predicted to have juxtamembrane coiled-coil dimers at high confidence (>95% in one heptad register, in some cases). Also, more BTN proteins are predicted to have coiled-coil dimers, compared with BTNL proteins (Figs. 7, 9). BTN/BTNL proteins with shorter juxtamembrane regions, such as BTN1A1h/m, BTNL3h, and BTNL8h, are not predicted to have coiled-coil dimers, although these proteins did have the conserved exon corresponding to BTN3A1 exon 5 that could potentially be a short dimerization motif in lieu of a longer coiled-coil dimer. BTNL proteins that have longer juxtamembrane regions but not predicted to have coiled-coil dimers (such as BTNL1m, BTNL6m, BTNL3h, and BTNL8h) need to form heteromeric complexes to function (40, 81, 82) so it is possible that they form heterodimeric coiled-coil dimers that cannot be predicted with existing programs.

Models of BTN3A1 structure were made based on the presence of a coiled-coil dimer and α helices and the two different crystal structures for BTN3A1 B30.2 dimers (34, 36, 66). In the extended model, the initial juxtamembrane segment is a coiled-coil dimer ending at exon 5 as two α helices that extend to the dimerization segment (exon 9) of the BTN3A1 B30.2 domains, as in the 4V1P and 4N7I structures (Fig. 10A). In the compact model, the initial juxtamembrane segment is again a coiled-coil dimer whose end in exon 5 overlaps the α helix of the alternate 5HM7 B30.2 dimer structure (Fig. 10A). However, for this structure to exist, the angle between the dimerization domain and the proximal α helix region would need to be less acute to prevent steric clash with the coiled-coil dimer. Also, the location of the proximal α helix prevents dimerization of the B30.2 domains through the dimerization segment. As noted above, the 5HM7 B30.2 structure confirms the presence of the distal α helix and the gap/bend between residues 291 and 293. Converting between the two states would require disrupting exon 9 dimerization and rotating the B30.2 domain upwards towards the cell membrane.

Other proteins use coiled-coil dimers for similar functions as those proposed for BTN3A1. B30.2 domains in TRIM proteins are positioned over coiled-coil dimers (83–85). These proteins are abundant and present in both vertebrates and invertebrates (86). Besides functioning in development and cell growth, many TRIM proteins function in immunity by enhancing innate immune responses at multiple levels in the signaling process (87, 88). TRIM proteins are dimerized by antiparallel coiled-coil dimers, and many have B30.2/PRY-

SPRY domains (86, 89, 90). The coiled-coil dimers position binding domains at the ends of the proteins while short disordered linkers position the B30.2 domains over the center of the coiled-coil dimer (83–85). Similar to the proposed BTN3A1 structure, Rho-associated, coiled-coil containing kinase contain a homodimeric parallel coiled-coil stalk with two globular kinase domains at its end (91). The kinesin motor protein, nonclaret disjunction, also uses a homodimeric parallel coiled-coil dimer as a “neck” to orient and link the two catalytic subunits on microtubules (92). Thus, similar to what is proposed for BTN3A1, several classes of proteins use parallel coiled-coil dimers as stalks with globular domains present at their ends (41).

How might coiled-coil dimers function in BTN3A1 sensing? Several possibilities can be proposed based on the function of coiled-coil dimers in other proteins (46). First, the coiled-coil dimers of BTN3 proteins may function as molecular spacers. In evolutionary studies, the lengths of coiled-coil regions in eukaryotic orthologous proteins are ~8-fold more conserved than the lengths of their non-coiled-coil regions (53). Insertions and deletions are also less likely to occur in coiled-coil dimers than in other parts of a protein (53). The lengths of coiled-coil dimers in orthologous proteins are more highly conserved than their sequences (53). The coiled-coil dimers of BTN3 proteins show similar evidence that they are functioning as molecular spacers. Whereas the IgV, IgC, and B30.2 domains are highly conserved between BTN3 family members and species (averaging 75, 80, and 81% identity, respectively, Supplemental Fig. 2), the coiled-coil dimers are only 39% conserved (Supplemental Fig. 3I, 3J). This difference is clearly demonstrated in exon 4, where the extracellular and transmembrane regions of the exon are 85% conserved, whereas the coiled-coil dimer of the exon is 36% conserved (Supplemental Fig. 3C–F). However, the predicted lengths for all of the BTN3 coiled-coil dimers by the MARCOIL program are similar (Fig. 1, Supplemental Fig. 1). Moreover, while “a” and “d” anchor residues are 58.3% identical between human BTN3A3 and alpaca and dolphin BTN3A3, “b,” “c,” “e,” “f,” and “g” residues are 41.4% identical. This difference in conservation is similar to that observed for proteins that use coiled-coil dimers as spacers (93). In contrast, coiled-coil dimers in proteins that have extensive contacts with other proteins or with other coiled-coil dimers differ because they conserve both anchor and nonanchor residues (the nonanchor residues are oriented to the outside of the coiled-coil interface) (93). Based on the differences in sequence conservation between the different domains of BTN3 proteins, it is likely that one function of the coiled-coil dimers of BTN3 proteins is to act as molecular spacers.

Another possible function for the coiled-coil dimer of BTN3A1 is to serve as a binding site for RhoB. RhoB and the closely-related RhoA and RhoC (~85% sequence identity), are small GTPases that act as molecular switches. They bind to other effector proteins for their function and play pivotal roles in the control of the actin cytoskeleton and in determining cell morphology. RhoB is required for the optimal stimulation of Vγ2Vδ2 T cells (94). Treatment of cancer cells with aminobisphosphonates leads to the redistribution of RhoB from the nucleus to BTN3A1 (94). This is associated with a reduction in the mobility of the BTN3A1 protein. RhoB directly binds to BTN3A1 through its juxtamembrane region (94). However, the exact binding site on BTN3A1 has not been determined.

Rho family members bind to specific effector proteins including serine/threonine protein kinases and scaffold proteins (95, 96). Rho binding domains have been divided into three types based on sequence/structural homology (95, 97). The domains bind to the same general region on Rho proteins but differ in some of the contact residues. These contact residues are conserved between RhoA, RhoB, and RhoC, and thus each can potentially bind a similar array of effector proteins. Two of the three types of binding sites are coiled-coil dimers. Binding to protein kinase C-related kinase 1, rhophilin, and rhotekin is through anti-parallel coiled-coil fingers (98, 99). In vitro Rho binding to Rho-associated, coiled-coil containing kinase 1/2, citron, and citron kinase is through parallel coiled-coil segments (100, 101), although this is controversial because binding may not take place in vivo (91). We speculate that the coiled-coil dimer of BTN3A1 might interact with RhoB, perhaps at exon 5/6, which is critical for the activity of BTN3A1 and conserved between BTN3 family members (36).

Several models can be proposed for how sensing of prenyl pyrophosphates leads to stimulation of Vγ2Vδ2 T cells (Fig. 10B). In model 1, BTN3A1 functions as both the sensor for prenyl pyrophosphates and the ligand for the Vγ2Vδ2 TCR. This could be due to a large rotational movement of the B30.2 domains that disrupts their dimerization and leads to conformational changes in the extracellular domains of BTN3A1 (Fig. 10B, model 1a). This level of alteration in BTN3A1 structure would be consistent with the large conformational changes noted in the juxtamembrane domain on HMBPP binding by the Weimer lab (39). Besides the juxtamembrane domain (35), the binding of prenyl pyrophosphates to the B30.2 domain also alters its conformation (66, 102) in the V1 and V2 loops (37). However, these changes in the conformation of B30.2 are less extensive and would be more consistent with model 1b. Either of these changes in the intracellular conformation could extend to the extracellular domains of BTN3A1 via the coiled-coil dimer.

In model 2, BTN3A1 also functions as a sensor and ligand for Vγ2Vδ2 T cells but requires a second protein for activity. The Vγ2Vδ2 TCR then recognizes a conformational change in the extracellular domains of BTN3A1 or in the clustering at the cell membrane. Support for model 2 comes from experiments using somatic hamster-human hybrid CHO cells (33). CHO cells expressing only BTN3A1 and treated with the 20.1 mAb stimulate Vγ2Vδ2 TCR reporter cells. However, CHO cells treated with either HMBPP or zoledronic acid are unable to stimulate (33). In contrast, hybrid CHO cells with human chromosome 6 (where BTN3 genes are located), stimulate Vγ2Vδ2 TCR reporter cells not only with the 20.1 mAb but also with HMBPP or zoledronic acid (33). Similar results were obtained with somatic mouse-human hybrid cells with the *p* arm of human chromosome 6, where BTN3 genes are located (32). Because only BTN3A1 was transfected into the CHO cells, stimulation by the 20.1 mAb does not require another human protein(s) whereas stimulation by sensing exogenous HMBPP or endogenous IPP induced by zoledronic acid, does. These results are consistent with model 2 (Fig. 10B). The simplest mechanism of action for the second protein is that it is recruited by the intracellular domain of BTN3A1 upon prenyl pyrophosphate binding to B30.2 and then mimics 20.1 mAb binding to the IgV domain.

In model 3 that we favor, the ligand for the Vγ2Vδ2 TCR is not solely BTN3 but also involves another protein, either as a complex between the second protein and BTN3 or through binding of both to different locations on the Vγ2Vδ2 TCR. The B30.2 domains, positioned by coiled-coil dimers, function as sensors for HMBPP and IPP and upon binding, the domains signal to the surface for Vγ2Vδ2 TCR stimulation. However, besides binding of BTN3 to a portion of the Vγ2Vδ2 TCR, the other CDRs of the Vγ2Vδ2 TCR bind a second ligand. This model of stimulation has been recently proposed for murine BTNL1/6 heterodimer stimulation of murine intestinal Vγ7 T cells and for human BTNL3/8 stimulation of human Vγ1.4 (also termed Vγ4) T cells (103). In both cases, stimulation of γδ T cells by BTNL heterodimers requires sequences in the hypervariable 4 region of the Vγ chain that is outside of the normal binding face of αβ and γδ TCRs. They can also respond to ligands binding to the normal TCR Ag recognition site involving CDR1, CDR2, and/or CDR3 regions (103). However, it is not clear whether such binding is required for stimulation by BTNL molecules. For human Vγ2Vδ2 T cells, we previously found that residues in the CDR1, CDR2, and CDR3 regions of both the human Vγ2 and Vδ2 chains are required for stimulation by prenyl pyrophosphates—although largely independent of the exact CDR3δ sequence or length (26, 104–106). These findings suggest that both BTN3 binding and the recognition of a second ligand are required for sensor activation of Vγ2Vδ2 T cells.

Expression of BTN3A2 or BTN3A3 augments stimulation of Vγ2Vδ2 T cells by BTN3A1 in experimental models (36, 40). However, BTN3A1 expression in human cells deleted of all BTN3 genes partially restores the cell's ability to stimulate Vγ2Vδ2 T cells (40, 66). Thus, BTN3A1 by itself is necessary and sufficient to stimulate Vγ2Vδ2 T cells. This is consistent with the fact that alpacas and dolphins have only one BTN3 isoform (67, 68). Coexpression of BTN3A2 or BTN3A3 can increase surface expression of BTN3A1 perhaps by masking juxtamembrane endoplasmic reticulum retention motifs in BTN3 heterodimers thereby augmenting stimulation (40) and/or by forming coiled-coil heterodimers. Besides increasing expression, the extracellular domains of BTN3A2 and BTN3A3 are highly homologous to BTN3A1 and are likely to undergo changes identical to those in BTN3A1 upon B30.2 sensing of prenyl pyrophosphates as they do when bound by the 20.1 mAb (29). Taken together, BTN3A2 and BTN3A3 likely augment stimulation by BTN3A1 sensing by increasing BTN3A1 levels and by undergoing changes in their extracellular domain identical to BTN3A1, but are not absolutely required and, thus, do not appear to function as the second protein in model 2.

All models require "inside-out" signaling to stimulate Vγ2Vδ2 T cells through their Vγ2Vδ2 TCRs. In these models, inside-out signaling results either in a conformational change in the extracellular BTN3 IgV-IgC dimer or a change in BTN3A1 aggregation or membrane distribution. The action of the 20.1 mAb provides evidence for a conformational change in the extracellular domains of BTN3. BTN3 molecules form "V" shaped homo- and heterodimers by interacting through their IgC domains (31, 66). The 20.1 mAb is specific for an epitope on the outer face of the IgV domain of BTN3 proteins (31). Its binding to the IgV domain makes APC stimulatory for Vγ2Vδ2 T cells (29–31) and induces a 19-Å rotational shift in the BTN3A1 dimer (31). This altered conformation could be what is recognized by the Vγ2Vδ2 TCR. Further supporting the conformational change model, the

Adams laboratory found that intracellular IPP accumulation in pamidronate-treated APC decreases the fluorescence resonance energy transfer signal between the plasma membrane and either the 20.1 mAb or the 103.2 mAb (specific for the top of the IgV domain) (94). Moreover, introducing a disulfide bond between the IgC domains that would reduce their movement, decreased stimulation by the 20.1 mAb as well as by HMBPP and pamidronate (66). Given the activity of the 20.1 mAb in CHO BTN3A1 transfectants, these findings support the hypothesis that at least part of the Ag/ligand for the Vγ2Vδ2 TCR is an altered conformation of the BTN3 extracellular domains.

Other BTN and BTNL proteins may have similar structure to that proposed for BTN3A1. Most, but not all, BTN and BTNL proteins are predicted to form parallel coiled-coil dimers starting after the transmembrane segment and ending before the B30.2 domains. They also express the dimerization coiled-coil exon positioned immediately before the B30.2 domain. Consistent with a dimerization function, almost all of the BTN and BTNL proteins, including orthologous BTN1A1 proteins from chickens and frogs, conserve the tryptophan residue in this exon that we have shown is critical for the stability of the BTN3A1 B30.2 dimer. The binding sites of the B30.2 models, however, show differences in their shape and surface potential (Fig. 8). Given the homologies between BTN3A1 and other BTN and BTNL proteins, it is possible that they could function similarly as sensors for other intracellular components such as small metabolites or proteins. Thus far, whereas BTN3A1h/BTN3A2h or BTN3A3 heteromers are required for maximal stimulation of human Vγ2Vδ2 T cells (40), BTNL1m/BTNL6m heteromers have been shown to be required for development of murine gut epithelial γδ T cells bearing Vγ7 TCRs (81, 82) and BTNL3h/BTNL8h heteromers are required for stimulation of human gut Vγ1.4Vδ1 T cells (40, 81). However, it is unclear whether sensing of ligands by the B30.2 domains of the BTNL molecules results in similar inside-out signaling to alter stimulation of the γδ T cells specific for these heteromers. This type of sensing and inside-out signaling may be a common mechanism used by BTN/BTNL proteins to stimulate other γδ T cell subsets, providing an explanation for the activation of γδ T cells bearing different γδ TCRs and for the difficulties in identifying ligands for γδ T cells. Although structural verification is required to confirm their presence, coiled-coil dimers may play important roles in signaling for many BTN and BTNL proteins.

Supplementary Material

Refer to Web version on PubMed Central for supplementary material.

Acknowledgments

We thank Zhimei Fang for technical assistance. We thank Drs. Thomas Herrmann, Mohinder M. Karunakaran, and Ms. Alina S. Fichtner for helpful discussion. Some computations were performed at the Academic Center for Computing and Media Studies, Kyoto University. Some of the computational resources were provided through a High Performance Computing Infrastructure research project (project ID: hp160165).

This work was supported by Department of Veterans Affairs (Veterans Health Administration, Office of Research and Development, Biomedical Laboratory Research and Development) Grant 1 I01 BX000972–01A1, National Cancer Institute Grant P30CA086862 (Core Support), and the University of Iowa Carver College of Medicine Carver Medical Research Initiative Grant to C.T.M. C.T.M. is the Kelting Family Scholar in Rheumatology. The

content of this manuscript are solely the responsibility of the authors and do not necessarily represent the official views of the granting agencies.

Abbreviations used in this article:

BTN	butyrophilin
BTNL	butyrophilin-like
HMBPP	(*E*)-4-hydroxy-3-methyl-but-2-enyl pyrophosphate
IPP	isopentenyl pyrophosphate
MFI	mean fluorescence intensity
PDB	Protein Data Base
RMS	root-mean-square
shRNA	short hairpin RNA
siRNA	small interfering RNA
TRIM	tripartite motif-containing

References

1. Morita CT, Jin C, Sarikonda G, and Wang H. 2007 Nonpeptide antigens, presentation mechanisms, and immunological memory of human Vγ2Vδ2 T cells: discriminating friend from foe through the recognition of prenyl pyrophosphate antigens. Immunol. Rev 215:59–76. [PubMed: 17291279]
2. Hintz M, Reichenberg A, Altincicek B, Bahr U, Gschwind RM, Kollas A-K, Beck E, Wiesner J, Eberl M, and Jomaa H. 2001 Identification of (*E*)-4-hydroxy-3-methyl-but-2-enyl pyrophosphate as a major activator for human γδ T cells in *Escherichia coli*. FEBS Lett. 509:317–322. [PubMed: 11741609]
3. Puan K-J, Jin C, Wang H, Sarikonda G, Raker AM, Lee HK, Samuelson MI, Märker-Hermann E, Pasa-Tolic L, Nieves E, Giner J-L, Kuzuyama T, and Morita CT. 2007 Preferential recognition of a microbial metabolite by human Vγ2Vδ2 T cells. Int. Immunol 19:657–673. [PubMed: 17446209]
4. Dieli F, Troye-Blomberg M, Ivanyi J, Fournié JJ, Krensky AM, Bonneville M, Peyrat MA, Caccamo N, Sireci G, and Salerno A. 2001 Granulysin-dependent killing of intracellular and extracellular *Mycobacterium tuberculosis* by Vγ9/Vδ2 T lymphocytes. J. Infect. Dis 184:1082–1085. [PubMed: 11574927]
5. Marischen L, Wesch D, Schröder JM, Wiedow O, and Kabelitz D. 2009 Human γδ T cells produce the protease inhibitor and antimicrobial peptide elafin. Scand. J. Immunol 70:547–552. [PubMed: 19906197]
6. Dudal S, Turriere C, Bessoles S, Fontes P, Sanchez F, Liautard J, Liautard JP, and Lafont V. 2006 Release of LL-37 by activated human Vγ9Vδ2 T cells: a microbicidal weapon against *Brucella suis*. J. Immunol 177:5533–5539. [PubMed: 17015740]
7. Qaqish A, Huang D, Chen CY, Zhang Z, Wang R, Li S, Yang E, Lu Y, Larsen MH, Jacobs WR Jr., Qian L, Frencher J, Shen L, and Chen ZW. 2017 Adoptive transfer of phosphoantigen-specific γδ T cell subset attenuates *Mycobacterium tuberculosis* infection in nonhuman primates. J. Immunol 198:4753–4763. [PubMed: 28526681]
8. Gober H-J, Kistowska M, Angman L, Jenö P, Mori L, and De Libero G. 2003 Human T cell receptor γδ cells recognize endogenous mevalonate metabolites in tumor cells. J. Exp. Med 197:163–168. [PubMed: 12538656]

9. Idrees ASM, Sugie T, Inoue C, Murata-Hirai K, Okamura H, Morita CT, Minato N, Toi M, and Tanaka Y. 2013 Comparison of γδ T cell responses and farnesyl diphosphate synthase inhibition in tumor cells pretreated with zoledronic acid. Cancer Sci. 104:536–542. [PubMed: 23387443]
10. Tanaka Y, Iwasaki M, Murata-Hirai K, Matsumoto K, Hayashi K, Okamura H, Sugie T, Minato N, Morita CT, and Toi M. 2017 Anti-tumor activity and immunotherapeutic potential of a bisphosphonate prodrug. Sci. Rep 7:5987. [PubMed: 28729550]
11. Wilhelm M, Kunzmann V, Eckstein S, Reimer P, Weissinger F, Ruediger T, and Tony H-P. 2003 γδ T cells for immune therapy of patients with lymphoid malignancies. Blood 102:200–206. [PubMed: 12623838]
12. Kobayashi H, Tanaka Y, Shimmura H, Minato N, and Tanabe K. 2010 Complete remission of lung metastasis following adoptive immunotherapy using activated autologous γδ T-cells in a patient with renal cell carcinoma. Anticancer Res. 30:575–579. [PubMed: 20332473]
13. Nicol AJ, Tokuyama H, Mattarollo SR, Hagi T, Suzuki K, Yokokawa K, and Nieda M. 2011 Clinical evaluation of autologous *gamma delta* T cell-based immunotherapy for metastatic solid tumours. Br. J. Cancer 105:778–786. [PubMed: 21847128]
14. Nakajima J, Murakawa T, Fukami T, Goto S, Kaneko T, Yoshida Y, Takamoto S, and Kakimi K. 2010 A phase I study of adoptive immunotherapy for recurrent non-small-cell lung cancer patients with autologous γδ T cells. Eur. J. Cardiothorac. Surg 37:1191–1197. [PubMed: 20137969]
15. Sakamoto M, Nakajima J, Murakawa T, Fukami T, Yoshida Y, Murayama T, Takamoto S, Matsushita H, and Kakimi K. 2011 Adoptive immunotherapy for advanced non-small cell lung cancer using zoledronate-expanded γδT cells: a phase I clinical study. J. Immunother 34:202–211. [PubMed: 21304399]
16. Kakimi K, Matsushita H, Murakawa T, and Nakajima J. 2014 γδ T cell therapy for the treatment of non-small cell lung cancer. Transl. Lung Cancer Res. 3:23–33. [PubMed: 25806278]
17. Kobayashi H, Tanaka Y, Yagi J, Minato N, and Tanabe K. 2011 Phase I/II study of adoptive transfer of γδ T cells in combination with zoledronic acid and IL-2 to patients with advanced renal cell carcinoma. Cancer Immunol. Immunother 60:1075–1084. [PubMed: 21519826]
18. Tanaka Y, Morita CT, Tanaka Y, Nieves E, Brenner MB, and Bloom BR. 1995 Natural and synthetic non-peptide antigens recognized by human γδ T cells. Nature 375:155–158. [PubMed: 7753173]
19. Kunzmann V, Bauer E, and Wilhelm M. 1999 γ/δ T-cell stimulation by pamidronate. N. Engl. J. Med 340:737–738. [PubMed: 10068336]
20. Zhang Y, Cao R, Yin F, Lin F-Y, Wang H, Krysiak K, No J-H, Mukkamala D, Houlihan K, Li J, Morita CT, and Oldfield E. 2010 Lipophilic pyridinium bisphosphonates: potent γδ T cell stimulators. Angew Chem. Int. Ed 49:1136–1138.
21. Zhang Y, Zhu W, Liu YL, Wang H, Wang K, Li K, No JH, Ayong L, Gulati A, Pang R, Freitas-Junior L, Morita CT, and Oldfield E. 2013 Chemo-immunotherapeutic anti-malarials targeting isoprenoid biosynthesis. ACS Med. Chem. Lett 4:423–427. [PubMed: 23610597]
22. Wang H, Sarikonda G, Puan K-J, Tanaka Y, Feng J, Giner J-L, Cao R, Mönkkönen J, Oldfield E, and Morita CT. 2011 Indirect stimulation of human Vγ2Vδ2 T cells through alterations in isoprenoid metabolism. J. Immunol 187:5099–5113. [PubMed: 22013129]
23. Li J, Herold MJ, Kimmel B, Müller I, Rincon-Orozco B, Kunzmann V, and Herrmann T. 2009 Reduced expression of the mevalonate pathway enzyme farnesyl pyrophosphate synthase unveils recognition of tumor cells by Vγ9Vδ2 T cells. J. Immunol 182:8118–8124. [PubMed: 19494338]
24. Bukowski JF, Morita CT, Tanaka Y, Bloom BR, Brenner MB, and Band H. 1995 Vγ2Vδ2 TCR-dependent recognition of non-peptide antigens and Daudi cells analyzed by TCR gene transfer. J. Immunol 154:998–1006. [PubMed: 7529807]
25. Bukowski JF, Morita CT, and Brenner MB. 1999 Human γδ T cells recognize alkylamines derived from microbes, edible plants, and tea: implications for innate immunity. Immunity 11:57–65. [PubMed: 10435579]
26. Wang H, Fang Z, and Morita CT. 2010 Vγ2Vδ2 T cell receptor recognition of prenyl pyrophosphates is dependent on all CDRs. J. Immunol 184:6209–6222. [PubMed: 20483784]

27. Morita CT, Beckman EM, Bukowski JF, Tanaka Y, Band H, Bloom BR, Golan DE, and Brenner MB. 1995 Direct presentation of nonpeptide prenyl pyrophosphate antigens to human γδ T cells. Immunity 3:495–507. [PubMed: 7584140]
28. Sarikonda G, Wang H, Puan K-J, Liu X-H, Lee HK, Song Y, Distefano MD, Oldfield E, Prestwich GD, and Morita CT. 2008 Photoaffinity antigens for human γδ T cells. J. Immunol 181:7738–7750. [PubMed: 19017963]
29. Harly C, Guillaume Y, Nedellec S, Peigné C-M, Mönkkönen H, Mönkkönen J, Li J, Kuball J, Adams EJ, Netzer S, Déchanet-Merville J, Léger A, Herrmann T, Breathnach R, Olive D, Bonneville M, and Scotet E. 2012 Key implication of CD277/butyrophilin-3 (BTN3A) in cellular stress sensing by a major human γδ T-cell subset. Blood 120:2269–2279. [PubMed: 22767497]
30. Wang H, Henry O, Distefano MD, Wang YC, Räikkönen J, Mönkkönen J, Tanaka Y, and Morita CT. 2013 Butyrophilin 3A1 plays an essential role in prenyl pyrophosphate stimulation of human Vγ2Vδ2 T cells. J. Immunol 191:1029–1042. [PubMed: 23833237]
31. Palakodeti A, Sandstrom A, Sundaresan L, Harly C, Nedellec S, Olive D, Scotet E, Bonneville M, and Adams EJ. 2012 The molecular basis for modulation of human Vγ9Vδ2 T cell responses by CD277/butyrophilin-3 (BTN3A)-specific antibodies. J. Biol. Chem 287:32780–32790. [PubMed: 22846996]
32. Vavassori S, Kumar A, Wan GS, Ramanjaneyulu GS, Cavallari M, El Daker S, Beddoe T, Theodossis A, Williams NK, Gostick E, Price DA, Soudamini DU, Voon KK, Olivo M, Rossjohn J, Mori L, and De Libero G. 2013 Butyrophilin 3A1 binds phosphorylated antigens and stimulates human γδ T cells. Nat. Immunol 14:908–916. [PubMed: 23872678]
33. Riaño F, Karunakaran MM, Starick L, Li J, Scholz CJ, Kunzmann V, Olive D, Amslinger S, and Herrmann T. 2014 Vγ9Vδ2 TCR-activation by phosphorylated antigens requires butyrophilin 3 A1 (*BTN3A1*) and additional genes on human chromosome 6. Eur. J. Immunol 44:2571–2576. [PubMed: 24890657]
34. Sandstrom A, Peigné C-M, Léger A, Crooks JE, Konczak F, Gesnel M-C, Breathnach R, Bonneville M, Scotet E, and Adams EJ. 2014 The intracellular B30.2 domain of butyrophilin 3A1 binds phosphoantigens to mediate activation of human Vγ9Vδ2 T cells. Immunity 40:490–500. [PubMed: 24703779]
35. Hsiao C-HC, Lin X, Barney RJ, Shippy RR, Li J, Vinogradova O, Wiemer DF, and Wiemer AJ. 2014 Synthesis of a phosphoantigen prodrug that potently activates Vγ9Vδ2 T-lymphocytes. Chem. Biol 21:945–954. [PubMed: 25065532]
36. Rhodes DA, Chen HC, Price AJ, Keeble AH, Davey MS, James LC, Eberl M, and Trowsdale J. 2015 Activation of human γδ T cells by cytosolic interactions of BTN3A1 with soluble phosphoantigens and the cytoskeletal adaptor periplakin. J. Immunol 194:2390–2398. [PubMed: 25637025]
37. Wang H, and Morita CT. 2015 Sensor function for butyrophilin 3A1 in prenyl pyrophosphate stimulation of human Vγ2Vδ2 T cells. J. Immunol 195:4583–4594. [PubMed: 26475929]
38. Peigné C-M, Léger A, Gesnel M-C, Konczak F, Olive D, Bonneville M, Breathnach R, and Scotet E. 2017 The juxtamembrane domain of butyrophilin BTN3A1 controls phosphoantigen-mediated activation of human Vγ9Vδ2 T cells. J. Immunol 198:4228–4234. [PubMed: 28461569]
39. Nguyen K, Li J, Puthenveetil R, Lin X, Poe MM, Hsiao CC, Vinogradova O, and Wiemer AJ. 2017 The butyrophilin 3A1 intracellular domain undergoes a conformational change involving the juxtamembrane region. FASEB J. 31:4697–4706. [PubMed: 28705810]
40. Vantourout P, Laing A, Woodward MJ, Zlatareva I, Apolonia L, Jones AW, Snijders AP, Malim MH, and Hayday AC. 2018 Heteromeric interactions regulate butyrophilin (BTN) and BTN-like molecules governing γδ T cell biology. Proc. Natl. Acad. Sci. USA 115:1039–1044. [PubMed: 29339503]
41. Lupas AN, and Gruber M. 2005 The structure of α-helical coiled coils. Adv. Protein Chem 70:37–78. [PubMed: 15837513]
42. Wagschal K, Tripet B, Lavigne P, Mant C, and Hodges RS. 1999 The role of position a in determining the stability and oligomerization state of α-helical coiled coils: 20 amino acid stability coefficients in the hydrophobic core of proteins. Protein Sci. 8:2312–2329. [PubMed: 10595534]

43. Tripet B, Wagschal K, Lavigne P, Mant CT, and Hodges RS. 2000 Effects of side-chain characteristics on stability and oligomerization state of a *de novo*-designed model coiled-coil: 20 amino acid substitutions in position "d". J. Mol. Biol 300:377–402. [PubMed: 10873472]
44. Lupas A, Van Dyke M, and Stock J. 1991 Predicting coiled coils from protein sequences. Science 252:1162–1164. [PubMed: 2031185]
45. Rose A, and Meier I. 2004 Scaffolds, levers, rods and springs: diverse cellular functions of long coiled-coil proteins. Cell. Mol. Life Sci 61:1996–2009. [PubMed: 15316650]
46. Truebestein L, and Leonard TA. 2016 Coiled-coils: the long and short of it. BioEssays 38:903–916. [PubMed: 27492088]
47. Gáspári Z, and Nyitray L. 2011 Coiled coils as possible models of protein structure evolution. Biomol Concepts 2:199–210. [PubMed: 25962029]
48. Surkont J, and Pereira-Leal JB. 2015 Evolutionary patterns in coiled-coils. Genome Biol Evol 7:545–556. [PubMed: 25577198]
49. Smeal T, Angel P, Meek J, and Karin M. 1989 Different requirements for formation of Jun: Jun and Jun: Fos complexes. Genes Dev. 3:2091–2100. [PubMed: 2516828]
50. Busch SJ, and Sassone-Corsi P. 1990 Dimers, leucine zippers and DNA-binding domains. Trends Genet. 6:36–40. [PubMed: 2186528]
51. van Herpen REMA, Tjeertes JV, Mulders SAM, Oude Ophuis RJA, Wieringa B, and Wansink DG. 2006 Coiled-coil interactions modulate multimerization, mitochondrial binding and kinase activity of myotonic dystrophy protein kinase splice isoforms. FEBS J. 273:1124–1136. [PubMed: 16519679]
52. Esposito D, Koliopoulos MG, and Rittinger K. 2017 Structural determinants of TRIM protein function. Biochem. Soc. Trans 45:183–191. [PubMed: 28202672]
53. Surkont J, Diekmann Y, Ryder PV, and Pereira-Leal JB. 2015 Coiled-coil length: size does matter. Proteins 83:2162–2169. [PubMed: 26387794]
54. Delorenzi M, and Speed T. 2002 An HMM model for coiled-coil domains and a comparison with PSSM-based predictions. Bioinformatics 18:617–625. [PubMed: 12016059]
55. Fariselli P, Molinini D, Casadio R, and Krogh A, eds. 2007 Prediction of Structurally-Determined Coiled-Coil Domains with Hidden Markov Models. Springer, Berlin Heidelberg.
56. Bartoli L, Fariselli P, Krogh A, and Casadio R. 2009 CCHMM_PROF: a HMM-based coiled-coil predictor with evolutionary information. Bioinformatics 25:2757–2763. [PubMed: 19744995]
57. Trigg J, Gutwin K, Keating AE, and Berger B. 2011 Multicoil2: predicting coiled coils and their oligomerization states from sequence in the twilight zone. PLoS One 6:e23519. [PubMed: 21901122]
58. Drozdetskiy A, Cole C, Procter J, and Barton GJ. 2015 JPred4: a protein secondary structure prediction server. Nucleic Acids Res 43:W389–394. [PubMed: 25883141]
59. Wood CW, Bruning M, Ibarra AÁ, Bartlett GJ, Thomson AR, Sessions RB, Brady RL, and Woolfson DN. 2014 CCBuilder: an interactive web-based tool for building, designing and assessing coiled-coil protein assemblies. Bioinformatics 30:3029–3035. [PubMed: 25064570]
60. Fiser A, Do RKG, and Šali A. 2000 Modeling of loops in protein structures. Protein Sci. 9:1753–1773. [PubMed: 11045621]
61. Šali A, and Blundell TL. 1993 Comparative protein modelling by satisfaction of spatial restraints. J. Mol. Biol 234:779–815. [PubMed: 8254673]
62. Baker NA, Sept D, Joseph S, Holst MJ, and McCammon JA. 2001 Electrostatics of nanosystems: application to microtubules and the ribosome. Proc. Natl. Acad. Sci. USA 98:10037–10041. [PubMed: 11517324]
63. Lindorff-Larsen K, Piana S, Palmo K, Maragakis P, Klepeis JL, Dror RO, and Shaw DE. 2010 Improved side-chain torsion potentials for the Amber ff99SB protein force field. Proteins 78:1950–1958. [PubMed: 20408171]
64. Hornak V, Abel R, Okur A, Strockbine B, Roitberg A, and Simmerling C. 2006 Comparison of multiple Amber force fields and development of improved protein backbone parameters. Proteins 65:712–725. [PubMed: 16981200]

65. Wang J, Cieplak P, and Kollman PA. 2000 How well does a restrained electrostatic potential (RESP) model perform in calculating conformational energies of organic and biological molecules? J. Comput. Chem 21:1049–1074.
66. Gu S, Sachleben JR, Boughter CT, Nawrocka WI, Borowska MT, Tarrasch JT, Skiniotis G, Roux B, and Adams EJ. 2017 Phosphoantigen-induced conformational change of butyrophilin 3A1 (BTN3A1) and its implication on Vγ9Vδ2 T cell activation. Proc. Natl. Acad. Sci. USA 114:E7311–E7320. [PubMed: 28807997]
67. Karunakaran MM, Göbel TW, Starick L, Walter L, and Herrmann T. 2014 Vγ9 and Vδ2 T cell antigen receptor genes and butyrophilin 3 (BTN3) emerged with placental mammals and are concomitantly preserved in selected species like alpaca (*Vicugna pacos*). Immunogenetics 66:243–254. [PubMed: 24526346]
68. Fichtner AS, Karunakaran MM, Starick L, Truman RW, and Herrmann T. 2018 The armadillo (*Dasypus novemcinctus*): a witness but not a functional example for the emergence of the butyrophilin 3/Vγ9Vδ2 system in placental mammals. Front. Immunol 9:265. [PubMed: 29527206]
69. van Heeckeren WJ, Sellers JW, and Struhl K. 1992 Role of the conserved leucines in the leucine zipper dimerization motif of yeast GCN4. Nucleic Acids Res 20:3721–3724. [PubMed: 1641337]
70. Serrano L, Neira JL, Sancho J, and Fersht AR. 1992 Effect of alanine versus glycine in α-helices on protein stability. Nature 356:453–455. [PubMed: 1557131]
71. Lyu PC, Liff MI, Marky LA, and Kallenbach NR. 1990 Side chain contributions to the stability of alpha-helical structure in peptides. Science 250:669–673. [PubMed: 2237416]
72. Li C, Ching Han Chang C, Nagel J, Porebski BT, Hayashida M, Akutsu T, Song J, and Buckle AM. 2016 Critical evaluation of *in silico* methods for prediction of coiled-coil domains in proteins. Brief. Bioinform 17:270–282. [PubMed: 26177815]
73. Gruber M, Söding J, and Lupas AN. 2006 Comparative analysis of coiled-coil prediction methods. J. Struct. Biol 155:140–145. [PubMed: 16870472]
74. Chothia C, and Lesk AM. 1986 The relation between the divergence of sequence and structure in proteins. EMBO J. 5:823–826. [PubMed: 3709526]
75. Mason JM, and Arndt KM. 2004 Coiled coil domains: stability, specificity, and biological implications. ChemBioChem. 5:170–176. [PubMed: 14760737]
76. Pace CN, and Scholtz JM. 1998 A helix propensity scale based on experimental studies of peptides and proteins. Biophys. J 75:422–427. [PubMed: 9649402]
77. Ermolenko DN, Richardson JM, and Makhatadze GI. 2003 Noncharged amino acid residues at the solvent-exposed positions in the middle and at the C terminus of the α-helix have the same helical propensity. Protein Sci. 12:1169–1176. [PubMed: 12761387]
78. López-Llano J, Campos LA, and Sancho J. 2006 α-helix stabilization by alanine relative to glycine: roles of polar and apolar solvent exposures and of backbone entropy. Proteins 64:769–778. [PubMed: 16755589]
79. Wilman HR, Shi J, and Deane CM. 2014 Helix kinks are equally prevalent in soluble and membrane proteins. Proteins 82:1960–1970. [PubMed: 24638929]
80. Hall SE, Roberts K, and Vaidehi N. 2009 Position of helical kinks in membrane protein crystal structures and the accuracy of computational prediction. J. Mol. Graph. Model 27:944–950. [PubMed: 19285892]
81. Di Marco Barros R, Roberts NA, Dart RJ, Vantourout P, Jandke A, Nussbaumer O, Deban L, Cipolat S, Hart R, Iannitto ML, Laing A, Spencer-Dene B, East P, Gibbons D, Irving PM, Pereira P, Steinhoff U, and Hayday A. 2016 Epithelia use butyrophilin-like molecules to shape organ-specific γδ T cell compartments. Cell 167:203–218. [PubMed: 27641500]
82. Lebrero-Fernández C, Bergström JH, Pelaseyed T, and Bas-Forsberg A. 2016 Murine Butyrophilin-Like 1 and Btnl6 form heteromeric complexes in small intestinal epithelial cells and promote proliferation of local T lymphocytes. Front. Immunol 7:1. [PubMed: 26834743]
83. Weinert C, Morger D, Djekic A, Grütter MG, and Mittl PR. 2015 Crystal structure of TRIM20 C-terminal coiled-coil/B30.2 fragment: implications for the recognition of higher order oligomers. Sci. Rep 5:10819. [PubMed: 26043233]

84. Sanchez JG, Okreglicka K, Chandrasekaran V, Welker JM, Sundquist WI, and Pornillos O. 2014 The tripartite motif coiled-coil is an elongated antiparallel hairpin dimer. Proc. Natl. Acad. Sci. USA 111:2494–2499. [PubMed: 24550273]

85. Li Y, Wu H, Wu W, Zhuo W, Liu W, Zhang Y, Cheng M, Chen YG, Gao N, Yu H, Wang L, Li W, and Yang M. 2014 Structural insights into the TRIM family of ubiquitin E3 ligases. Cell Res. 24:762–765. [PubMed: 24722452]

86. Sardiello M, Cairo S, Fontanella B, Ballabio A, and Meroni G. 2008 Genomic analysis of the TRIM family reveals two groups of genes with distinct evolutionary properties. BMC Evol. Biol 8:225. [PubMed: 18673550]

87. Versteeg GA, Rajsbaum R, Sánchez-Aparicio MT, Maestre AM, Valdiviezo J, Shi M, Inn K-S, Fernandez-Sesma A, Jung J, and García-Sastre A. 2013 The E3-ligase TRIM family of proteins regulates signaling pathways triggered by innate immune pattern-recognition receptors. Immunity 38:384–398. [PubMed: 23438823]

88. Versteeg GA, Benke S, García-Sastre A, and Rajsbaum R. 2014 InTRIMsic immunity: Positive and negative regulation of immune signaling by tripartite motif proteins. Cytokine Growth Factor Rev. 25:563–576. [PubMed: 25172371]

89. Reymond A, Meroni G, Fantozzi A, Merla G, Cairo S, Luzi L, Riganelli D, Zanaria E, Messali S, Cainarca S, Guffanti A, Minucci S, Pelicci PG, and Ballabio A. 2001 The tripartite motif family identifies cell compartments. EMBO J. 20:2140–2151. [PubMed: 11331580]

90. Rhodes DA, de Bono B, and Trowsdale J. 2005 Relationship between SPRY and B30.2 protein domains. Evolution of a component of immune defence? Immunology 116:411–417. [PubMed: 16313355]

91. Truebestein L, Elsner DJ, Fuchs E, and Leonard TA. 2015 A molecular ruler regulates cytoskeletal remodelling by the Rho kinases. Nat. Commun 6:10029. [PubMed: 26620183]

92. Sablin EP, Case RB, Dai SC, Hart CL, Ruby A, Vale RD, and Fletterick RJ. 1998 Direction determination in the minus-end-directed kinesin motor ncd. Nature 395:813–816. [PubMed: 9796817]

93. White GE, and Erickson HP. 2006 Sequence divergence of coiled coils--structural rods, myosin filament packing, and the extraordinary conservation of cohesins. J. Struct. Biol 154:111–121. [PubMed: 16495084]

94. Sebestyen Z, Scheper W, Vyborova A, Gu S, Rychnavska Z, Schiffler M, Cleven A, Chéneau C, van Noorden M, Peigné C-M, Olive D, Lebbink RJ, Oostvogels R, Mutis T, Schuurhuis GJ, Adams EJ, Scotet E, and Kuball J. 2016 RhoB mediates phosphoantigen recognition by Vγ9Vδ2 T cell receptor. Cell Rep. 15:1973–1985. [PubMed: 27210746]

95. Bishop AL, and Hall A. 2000 Rho GTPases and their effector proteins. Biochem. J 348 Pt 2:241–255. [PubMed: 10816416]

96. Kühn S, and Geyer M. 2014 Formins as effector proteins of Rho GTPases. Small GTPases 5:e29513. [PubMed: 24914801]

97. Rose R, Weyand M, Lammers M, Ishizaki T, Ahmadian MR, and Wittinghofer A. 2005 Structural and mechanistic insights into the interaction between Rho and mammalian Dia. Nature 435:513–518. [PubMed: 15864301]

98. Maesaki R, Ihara K, Shimizu T, Kuroda S, Kaibuchi K, and Hakoshima T. 1999 The structural basis of Rho effector recognition revealed by the crystal structure of human RhoA complexed with the effector domain of PKN/PRK1. Mol. Cell 4:793–803. [PubMed: 10619026]

99. Hutchinson CL, Lowe PN, McLaughlin SH, Mott HR, and Owen D. 2011 Mutational analysis reveals a single binding interface between RhoA and its effector, PRK1. Biochemistry 50:2860–2869. [PubMed: 21351730]

100. Dvorsky R, Blumenstein L, Vetter IR, and Ahmadian MR. 2004 Structural insights into the interaction of ROCKI with the switch regions of RhoA. J. Biol. Chem 279:7098–7104. [PubMed: 14660612]

101. Julian L, and Olson MF. 2014 Rho-associated coiled-coil containing kinases (ROCK): structure, regulation, and functions. Small GTPases 5:e29846. [PubMed: 25010901]

102. Salim M, Knowles TJ, Baker AT, Davey MS, Jeeves M, Sridhar P, Wilkie J, Willcox CR, Kadri H, Taher TE, Vantourout P, Hayday A, Mehellou Y, Mohammed F, and Willcox BE. 2017 BTN3A1

discriminates γδ T cell phosphoantigens from nonantigenic small molecules via a conformational sensor in its B30.2 domain. ACS Chem. Biol 12:2631–2643. [PubMed: 28862425]

103. Melandri D, Zlatareva I, Chaleil RAG, Dart RJ, Chancellor A, Nussbaumer O, Polyakova O, Roberts NA, Wesch D, Kabelitz D, Irving PM, John S, Mansour S, Bates PA, Vantourout P, and Hayday AC. 2018 The γδ TCR combines innate immunity with adaptive immunity by utilizing spatially distinct regions for agonist selection and antigen responsiveness. Nat. Immunol 19:1352–1365. [PubMed: 30420626]
104. Bukowski JF, Morita CT, Band H, and Brenner MB. 1998 Crucial role of TCRγ chain junctional region in prenyl pyrophosphate antigen recognition by γδ T cells. J. Immunol 161:286–293. [PubMed: 9647235]
105. Miyagawa F, Tanaka Y, Yamashita S, Mikami B, Danno K, Uehara M, and Minato N. 2001 Essential contribution of germline-encoded lysine residues in Jγ1.2 segment to the recognition of nonpeptide antigens by human γδ T cells. J. Immunol 167:6773–6779. [PubMed: 11739492]
106. Yamashita S, Tanaka Y, Harazaki M, Mikami B, and Minato N. 2003 Recognition mechanism of non-peptide antigens by human γδ T cells. Int. Immunol 15:1301–1307. [PubMed: 14565928]

Key Points

- Part of the juxtamembrane of butyrophilin 3A1 proteins forms a coiled-coil dimer
- The coiled-coil dimer is critical for BTN3A1 stimulation of Vγ2Vδ2 T cells
- B30.2 domains of BTN3A1 proteins also dimerize through a short coiled-coil region

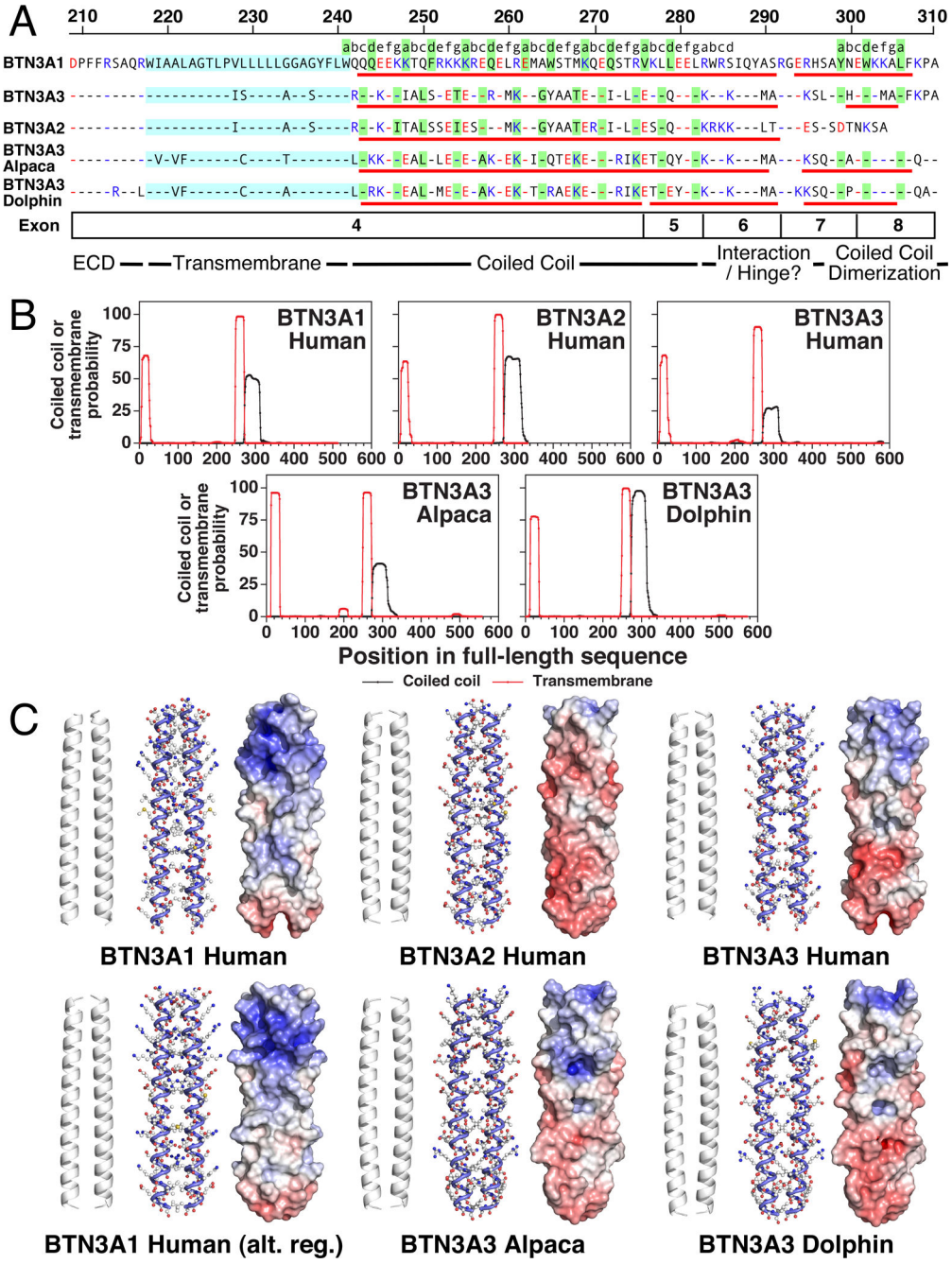

FIGURE 1.

Coiled-coil dimers are predicted for all BTN3 proteins in their juxtamembrane segments immediately following their transmembrane segments. (**A**) Sequence of the juxtamembrane segments of BTN3 proteins. Residues predicted to form transmembrane regions are shaded cyan. Residues predicted to form an α helix are underlined in red with the gaps representing gaps/bends in the helix. The gap in BTN3A1 is based on the alternate B30.2 dimer structure (5HM7) whereas the BTN3A3 and BTN3A2 α helices are predicted by the JPred4 program. Residues predicted to be anchor residues (“a” or “d” positions) for coiled-coil dimers are shaded green. Basic residues are colored blue and acidic residues are colored red. Exon

locations and their proposed functions are shown for BTN3A1 below the sequences. Numbering starts are residue 31 of the full length BTN3A1 protein. Note that two heptad registers are predicted for alpaca BTN3A3 with approximately equal probabilities and the one corresponding to human BTN3A2/BTN3A3 is shown. (**B**) Probability of coiled-coil and transmembrane regions in BTN3 proteins. Numbering is for the full-length protein including the signal peptide. The coiled-coil dimer probability is plotted (black lines) for the register with the highest probability of forming a coiled-coil dimer, as predicted by the MARCOIL v1.0 program. The transmembrane region probability is plotted (red lines) as predicted by the TMHMM v2.0 program. Note that the coiled-coil dimers are all predicted to begin immediately after the transmembrane segment and are of similar length. (**C**) Models of the coiled-coil dimers of BTN3 proteins. Models of the coiled-coil dimers of BTN3 proteins. Models of the predicted coiled-coil dimers (full length residues 273–312) were made using the CCBuilder2 program. Models of human BTN3 proteins were optimized using the CCBuilder2 function. Cartoons (left), ball-and-stick models (middle), and the surface potentials (right) of the coiled-coil dimers (identically positioned) are shown, with the top of the structure being closest to the cell membrane. Surface potentials are colored from red (negative potential, −10 kT) to blue (positive potential, +10 kT). BTN3A1 alternative register model (lower left) is based with residue 273 at the “d” position rather than at the “c” position (upper left).

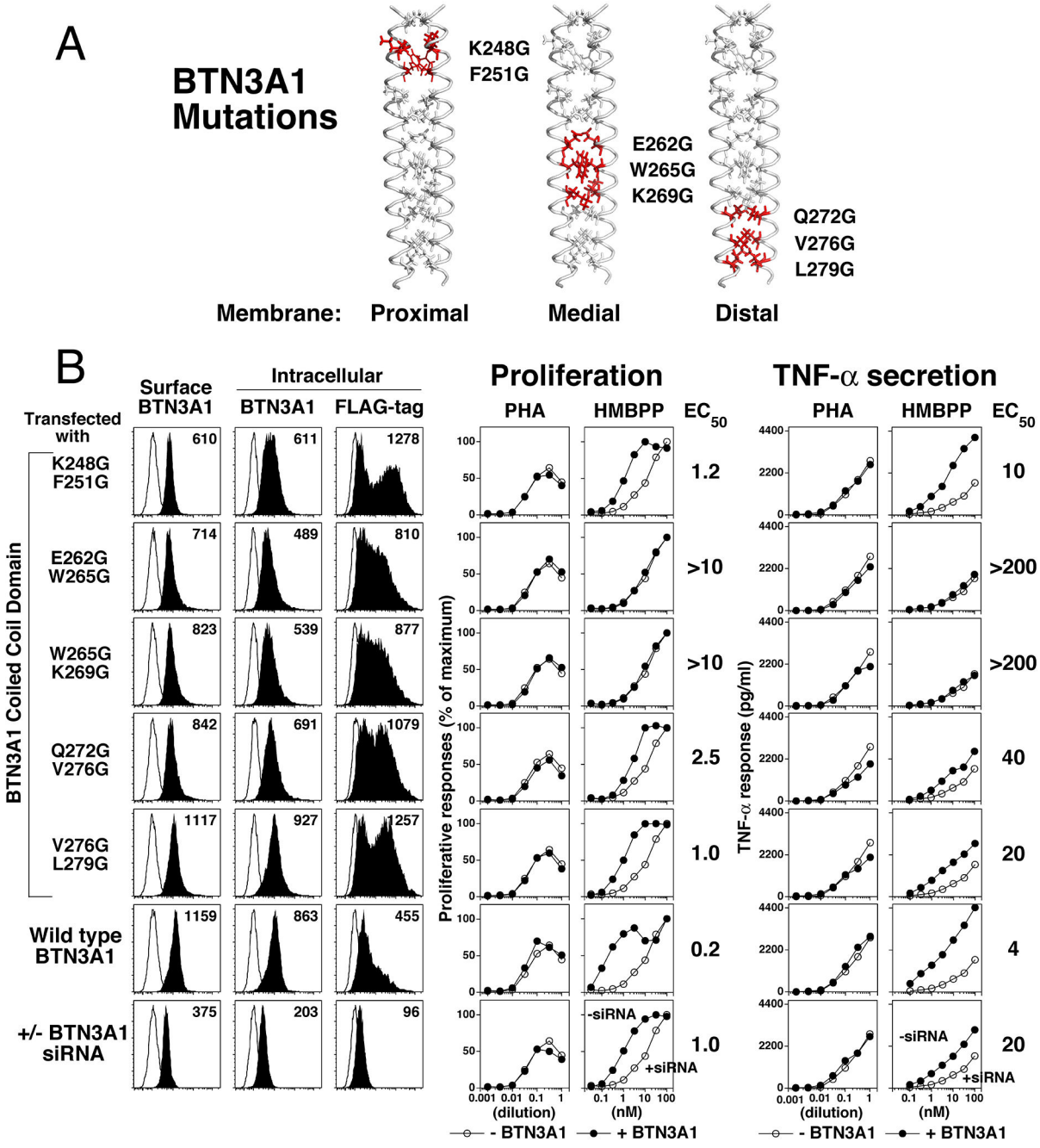

FIGURE 2.

Mutation of anchor residues in the intracellular juxtamembrane coiled-coil dimer of BTN3A1 can reduce or abrogate prenyl pyrophosphate stimulation of Vγ2Vδ2 T cells. (**A**) Location of anchor residue mutations in the predicted coiled-coil dimer of BTN3A1. Dual glycine mutations were made in BTN3A1 residues predicted to be adjacent “a” and “d” anchor residues for the coiled-coil dimer at sites that are proximal, medial, and distal to the transmembrane region. (**B**) BTN3 surface and intracellular expression by BTN3A1 siRNA-treated HeLa cells expressing mutant or wild-type BTN3A1 (*left panels*). Effect of mutations in BTN3A1 on proliferation (*middle panels*) and TNF-α secretion (*right panels*)

by Vγ2Vδ2 T cells in response to PHA or HMBPP. BTN3A1 residues predicted to anchor the coiled-coil dimer (the “a” and “d” positions) were mutated to glycine by site-directed mutagenesis at proximal, medial, and distal locations relative to the transmembrane region. Glycine mutation of two adjacent anchor residues would be predicted to locally destabilize the coiled-coil dimer. HeLa cells were transfected with a control siRNA, an siRNA specific for the 3’UT region of endogenous BTN3A1, or co-transfected with an siRNA specific for the 3’UT region of endogenous BTN3A1 and either a wild-type or mutant BTN3A1 cDNA. After 72 h, the transfectants were harvested and a portion stained with either PE-P3 IgG1 control mAb or PE-20.1 mAb on intact cells to measure surface expression. To assess intracellular expression, cells were permeabilized with saponin and stained with PE-P3 IgG1 control mAb, PE-20.1 mAb, or anti-FLAG mAb and analyzed using a LSR II flow cytometer (*left panels*). The relative MFI was calculated as 20.1 mAb MFI minus isotype control mAb MFI (shown on panels). The remaining cells were treated with mitomycin C and then cultured with 12G12 Vγ2Vδ2 T cells and the PHA mitogen or HMBPP. After 24 h, the supernatants were harvested and TNF-α levels determined by ELISA. The cells were pulsed with [^{3}H]-thymidine and harvested 18 h later. Because of differences in their plateau values, proliferative responses were normalized to set the HMBPP plateau values as 100%. The EC_{50} values are shown on the right. Note that the HeLa cells still expressed the BTN3A2 and BTN3A3 isoforms of BTN3 but lacked the critical BTN3A1 isoform. Representative of two experiments with singlicate dose response curves.

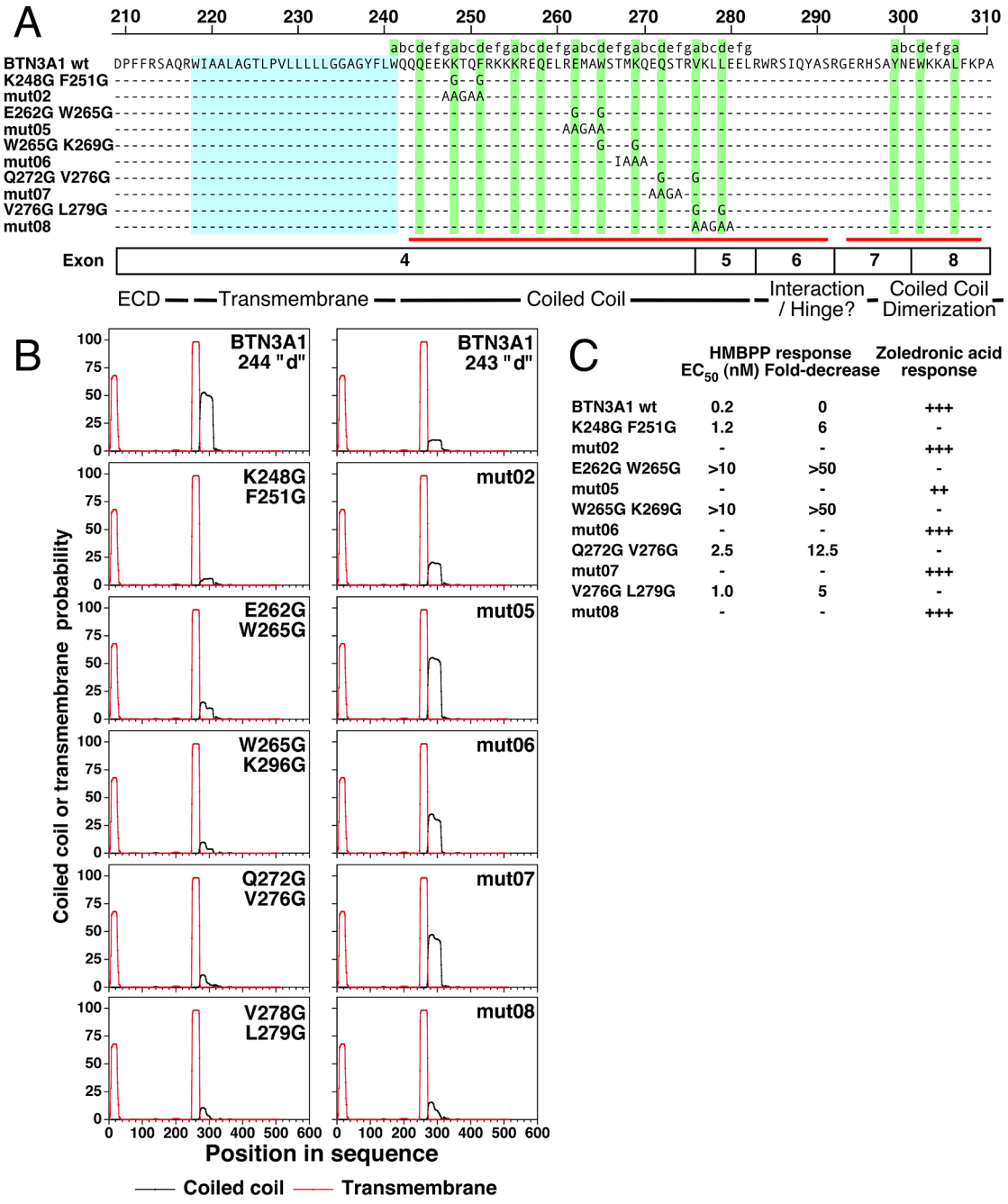

FIGURE 3.

Effect of mutations in the juxtamembrane region of BTN3A1 on coiled-coil dimer probability and stimulation of Vγ2Vδ2 T cells. (**A**) Location of mutations in the juxtamembrane of BTN3A1. Mutations were from this study and from the Scotet laboratory (38) (mut02-mut08). Shading, exon location, and numbering are as in Fig. 1B. Note that all mutant BTN3A1 proteins are predicted to form continuous α helices in their juxtamembrane regions despite glycine substitutions. (**B**) Mutations in BTN3A1 affect the probability of juxtamembrane coiled-coil dimers. Numbering is for the full-length protein including the signal peptide. Note that the glycine mutations are predicted to eliminate the coiled-coil

dimer. (**C**) Effect of mutations in the juxtamembrane region of BTN3A1 on stimulation of Vγ2Vδ2 T cells. HMBPP responses for mutations from this study and zoledronic acid responses for mutations from the Scotet laboratory (38) are shown. ++, 25–75% of control response; +++, >75% of control response.

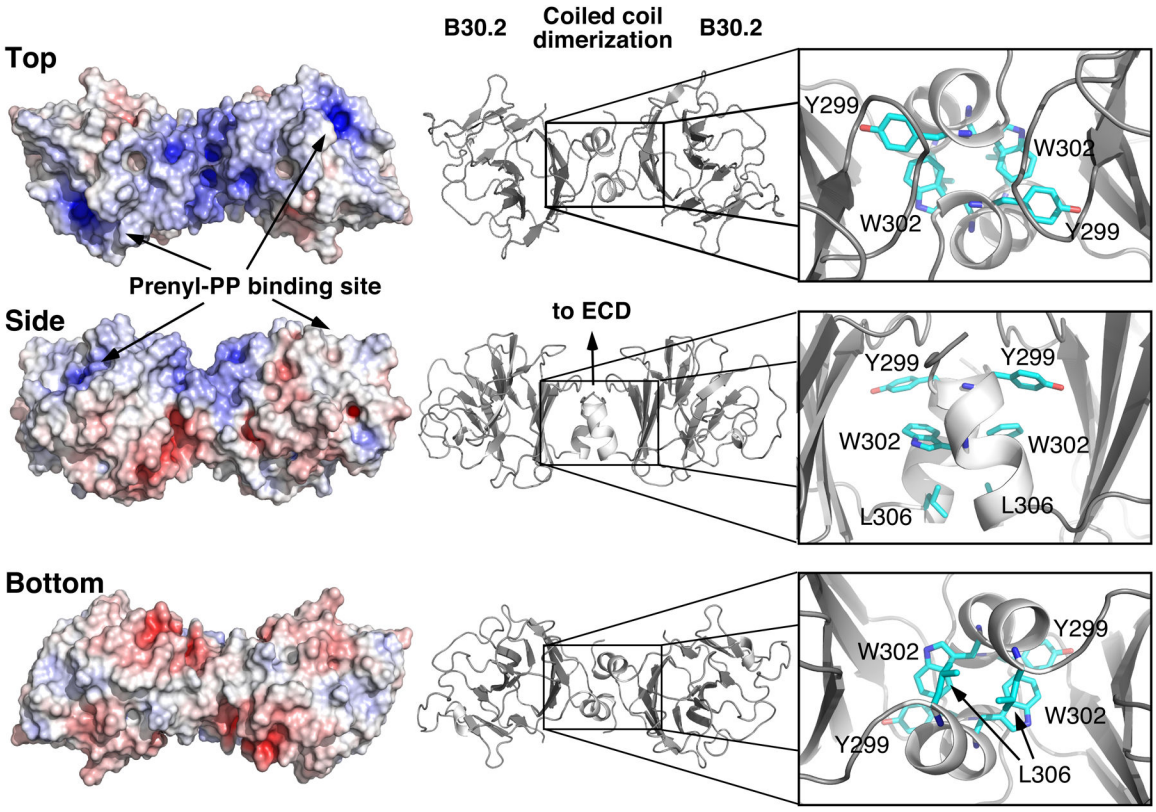

FIGURE 4.

Structure of the BTN3A1 B30.2 dimer and its coiled-coil dimerization interface. Surface potential of the BTN3A1 B30.2 dimer in top, side, and bottom orientations as viewed from the cell membrane (*left structures*). Surface potentials are colored from red (negative potential, −10 kT) to blue (positive potential, +10 kT). Cartoon views of the BTN3A1 B30.2 dimer as viewed in three orientations (*middle structures*). Close-up views of the dimerization interface with potential anchor residues shown as sticks (*right structures*).

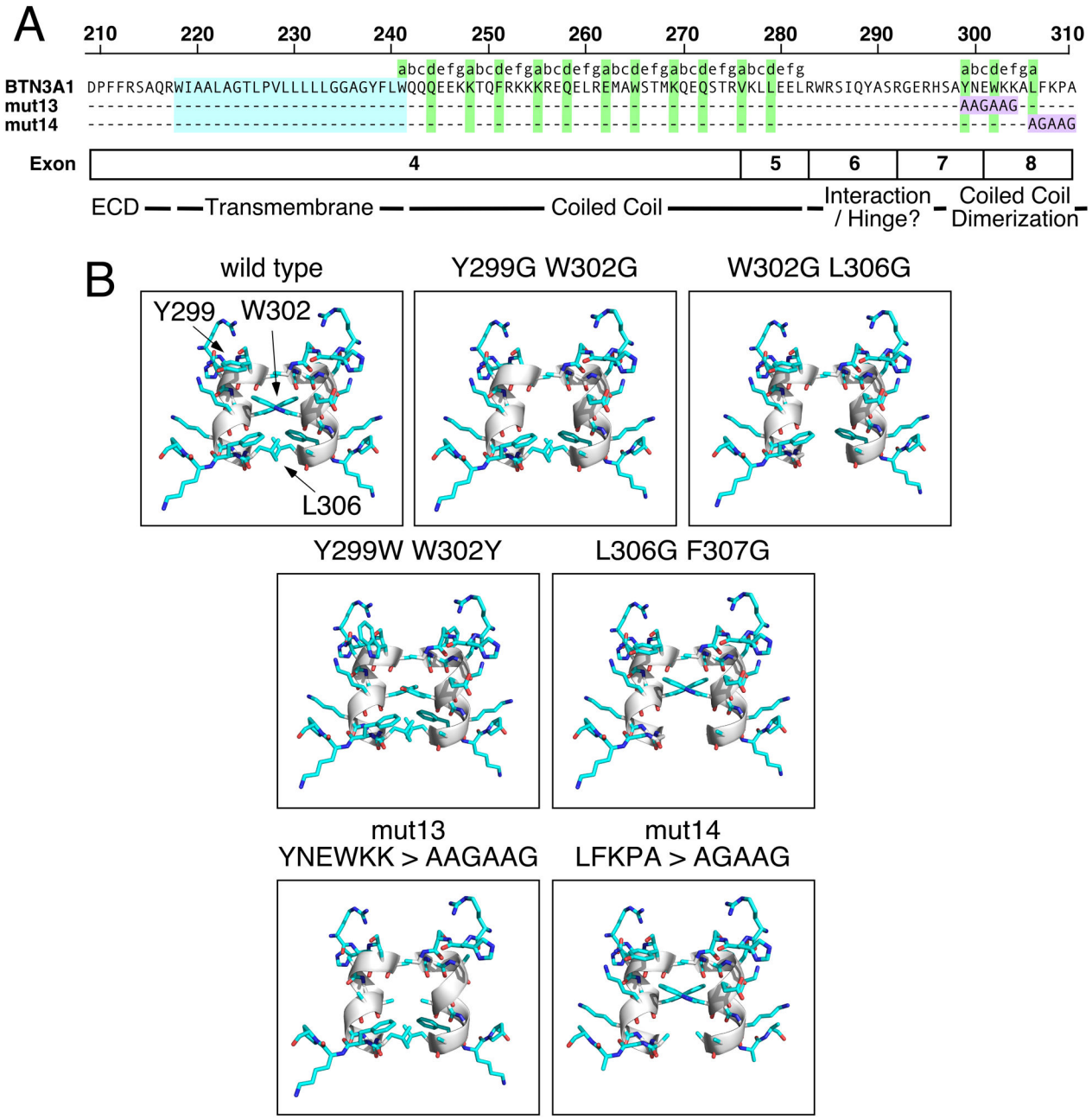

FIGURE 5.

Structures of BTN3A1 B30.2 dimers with mutations at the coiled-coil dimerization region. (**A**) Sequence of the juxtamembrane region of BTN3A1 showing the location of mut13 and mut14 aa differences. The mutated sequences are shaded purple. The transmembrane regions are shaded cyan and the predicted anchor residues are shaded green. (**B**) Structural models of BTN3A1 B30.2 dimers with mutations in the coiled-coil dimerization region. Close-up side views of the dimerization region are shown. The mutated residues are listed above each panel. Residues were mutated to the indicated amino acid in silico for the BTN3A1 B30.2 dimer structure (PDB 4V1P) using the Mutagenesis Wizard in PyMOL v1.8.6.2.

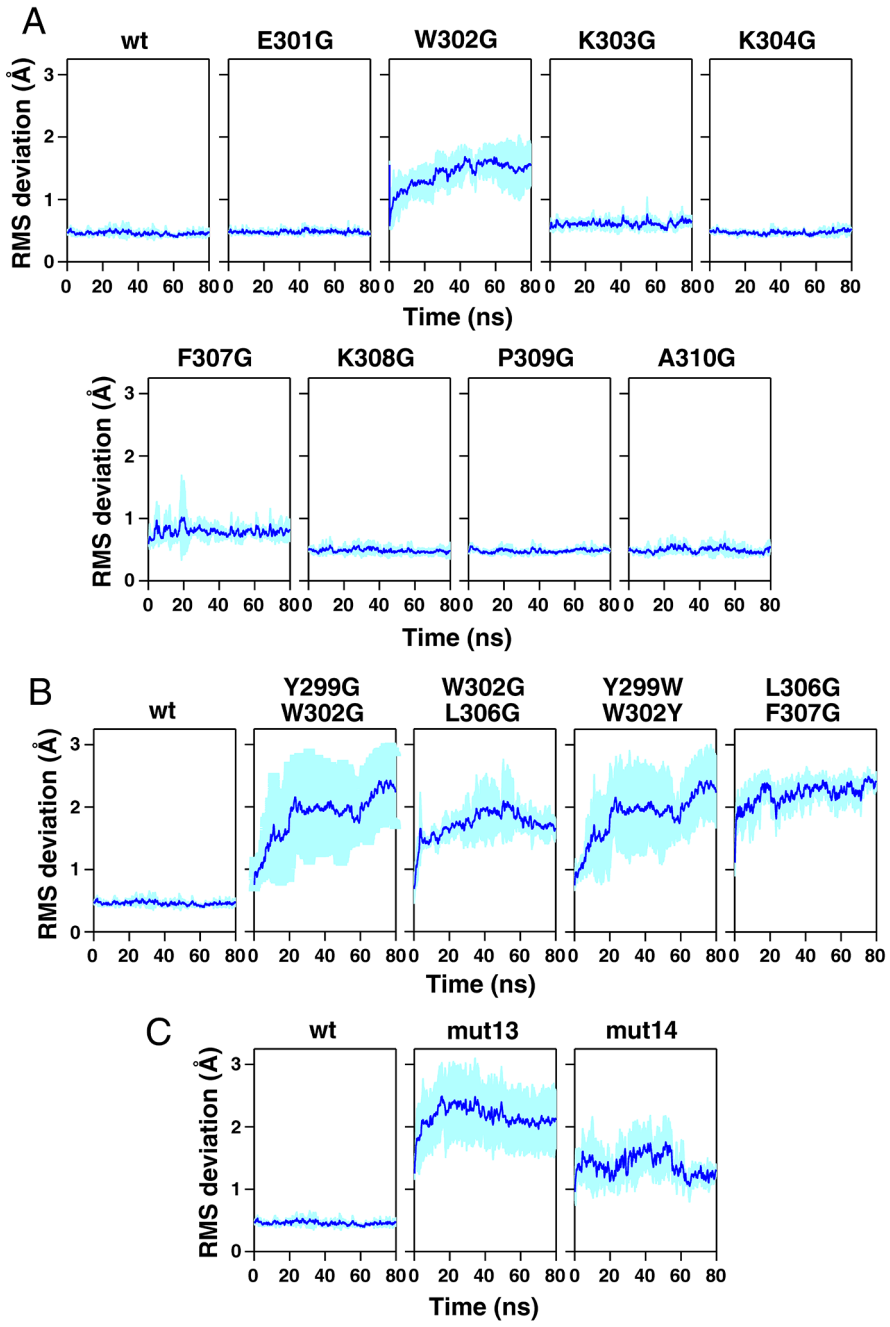

FIGURE 6.

Effect of mutations in the dimerization region on the predicted stability of BTN3A1 B30.2 dimers as assessed by the RMS differences of the Cα atoms of the helices of the BTN3A1 dimer. (A) Effect of single glycine mutations, (B) dual mutations, and (C) multiple mutations on the predicted stability of helices of the BTN3A1 B30.2 dimer. The mutations in the BTN3A1 B30.2 dimerization region corresponding to mut13 and mut14 were reported by the Scotet laboratory to abolish BTN3A1 mediated stimulation. Models of mutant dimers were based on the crystal structure of BTN3A1 B30.2 residues 295–483 of the mature protein (PDB 4V1P) and made using the MODELLER program. The stability of the mutant

BTN3A1 B30.2 dimers were then assessed by molecular dynamics simulations. Each panel shows the average RMS deviation of the Cα atoms of the helices calculated using the initial structure of the BTN3A1 B30.2 dimer as a reference for 80 ns for four replicate simulations. The average RMS deviation is plotted as a dark blue line with the SD shown as light blue shading.

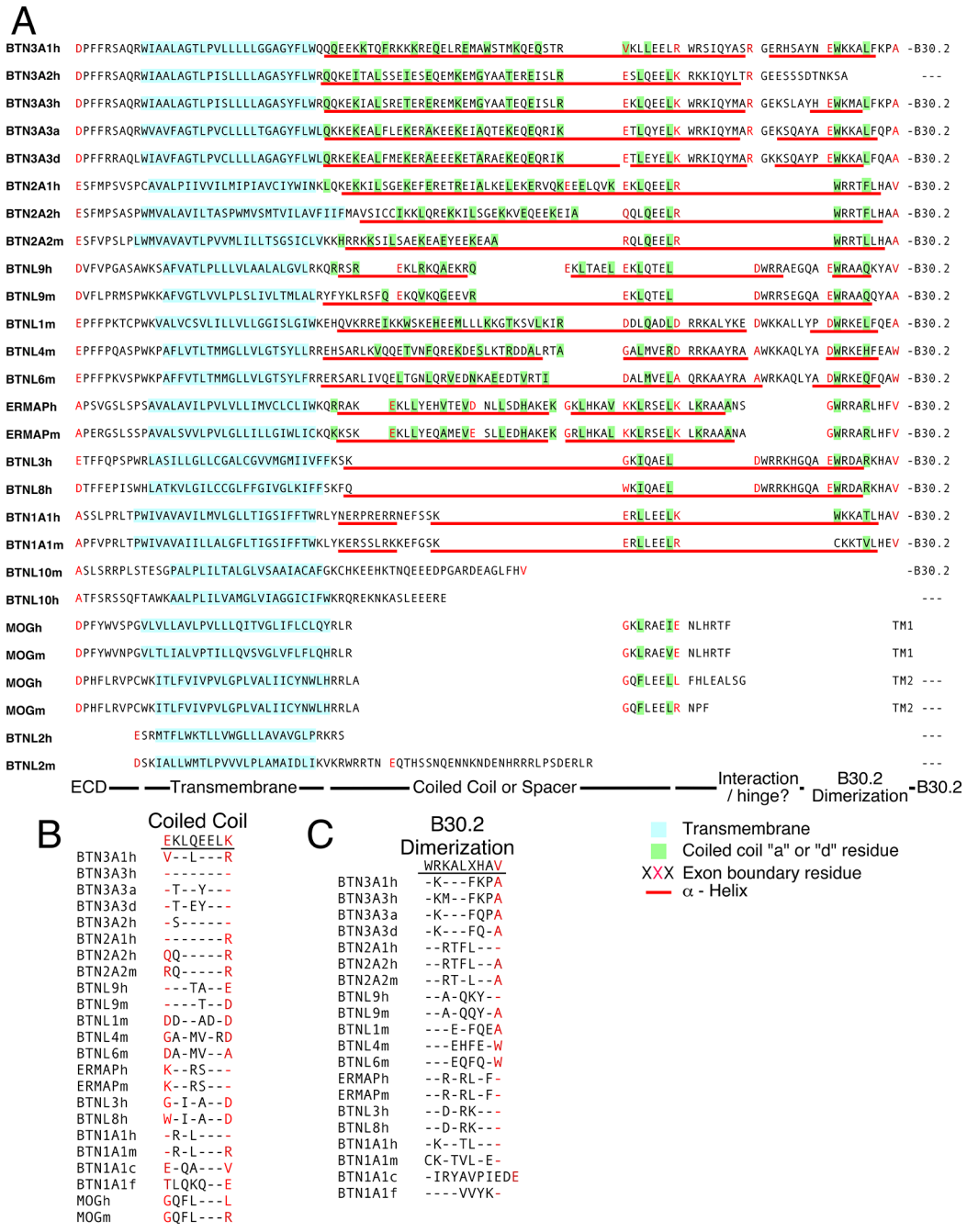

FIGURE 7.

Comparisons between the juxtamembrane segment of human and murine BTN and BTNL family proteins. (**A**) Sequence and exon boundaries of the juxtamembrane segment of human and murine BTN and BTNL family proteins. The sequence of the juxtamembrane regions is shown for the longest isoform for each protein. Amino acid residues highlighted in cyan are predicted to be part of the transmembrane domain. Amino acid residues highlighted in green are predicted to be anchor residues (“a” and “d” residues) in coiled-coil dimers with >18% probability. Amino acid residues colored red delineate the junctions between exons. Residues predicted to form an α helix are underlined in red with gaps

representing breaks in the helix. The extracellular domains are located on the left of the sequence whereas the B30.2 domains (if present) on the right. Note that all BTN and BTNL proteins with coiled-coil dimers are predicted to have α helices between the membrane and B30.2 with 0–2 gaps in the α helix, only 1 gap is due to a proline residue (BTNL1m). Also, BTNL10h may be a pseudogene. (**B**) Conserved juxtamembrane exon in BTN and BTNL proteins. This exon is found in all BTN and BTNL proteins except BTNL2 and BTNL10. The leucine residues at position 3 and 7 are highly conserved. (**C**) Exon encoding the dimerization region for BTN3A1 is conserved in all BTN and BTNL proteins with B30.2 domains. The exon immediately preceding the start of the B30.2 domain exon is conserved in all BTN and BTNL proteins with B30.2 domains (except for BTNL10m that may not be expressed and whose human ortholog lacks a B30.2 domain and is predicted to be a pseudogene). Note that all exons start with tryptophan except for BTN1A1m. c, chicken; f, frog (*Xenopus*); h, human; m, murine.

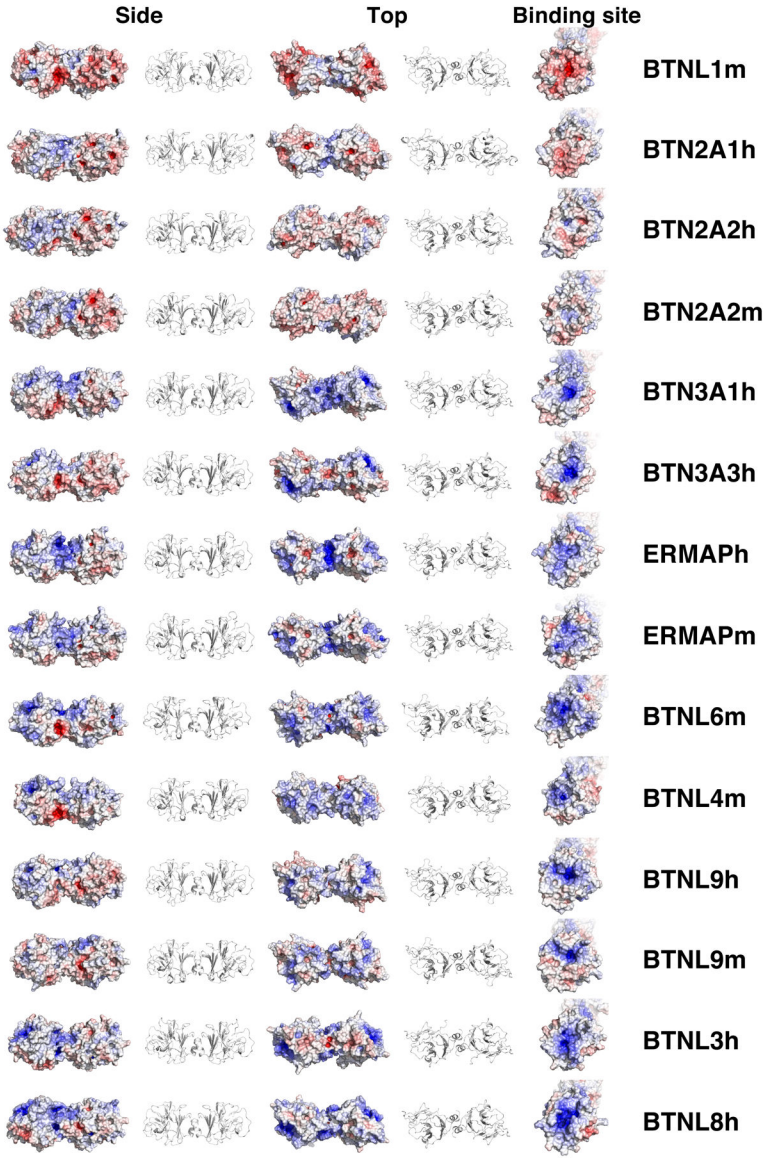

FIGURE 8.

Models of B30.2 dimers for human and murine BTN and BTNL proteins. BTN and BTNL B30.2 dimers were modeled using the MODELLER v2.0 plugin (PyMod 2.0) with Pymol 1.8.6.2. Surface potentials are colored from red (negative potential, −10 kT) to blue (positive potential, +10 kT).

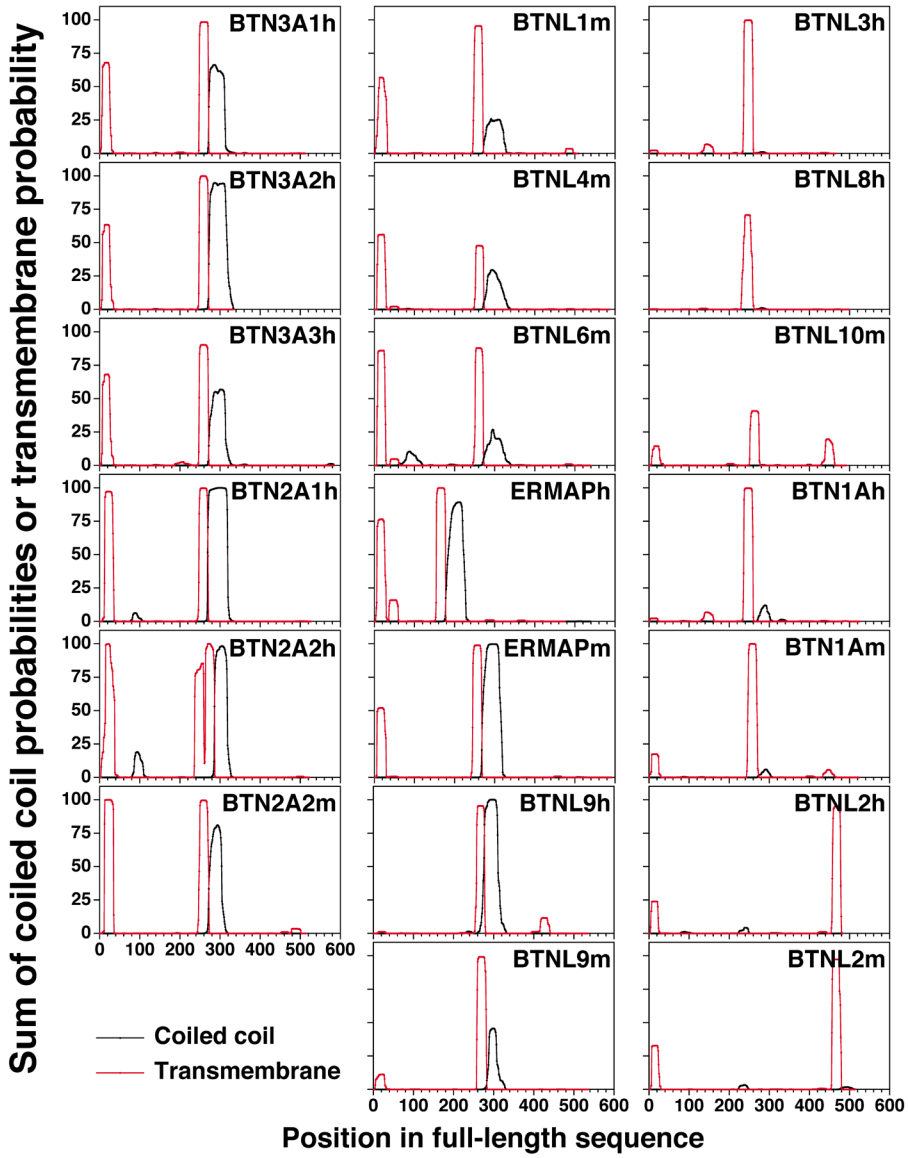

FIGURE 9.

Predicted locations of coiled-coil and transmembrane regions in human and murine butyrophilin and butyrophilin-like family proteins. The transmembrane region probability (red lines) and the sum of coiled-coil dimer probabilities (black lines) are shown for the longest predicted mRNA species for each protein. Numbering is for the full-length protein including the signal peptide. Leader and transmembrane regions were predicted by the TMHMM v2.0 program. The sum of probabilities in all registers that a residue is part of a coiled-coil dimer as predicted by the MARCOIL v1.0 program is plotted. Note that all coiled-coil domains are predicted to begin immediately after the end of the transmembrane regions and that coiled-coil dimer predictions are conserved between humans and mouse orthologs. BTN3 predictions are higher than those shown in Fig. 1A in which the probability of the best single register is shown rather than the sum of all registers. h, human; m, murine.

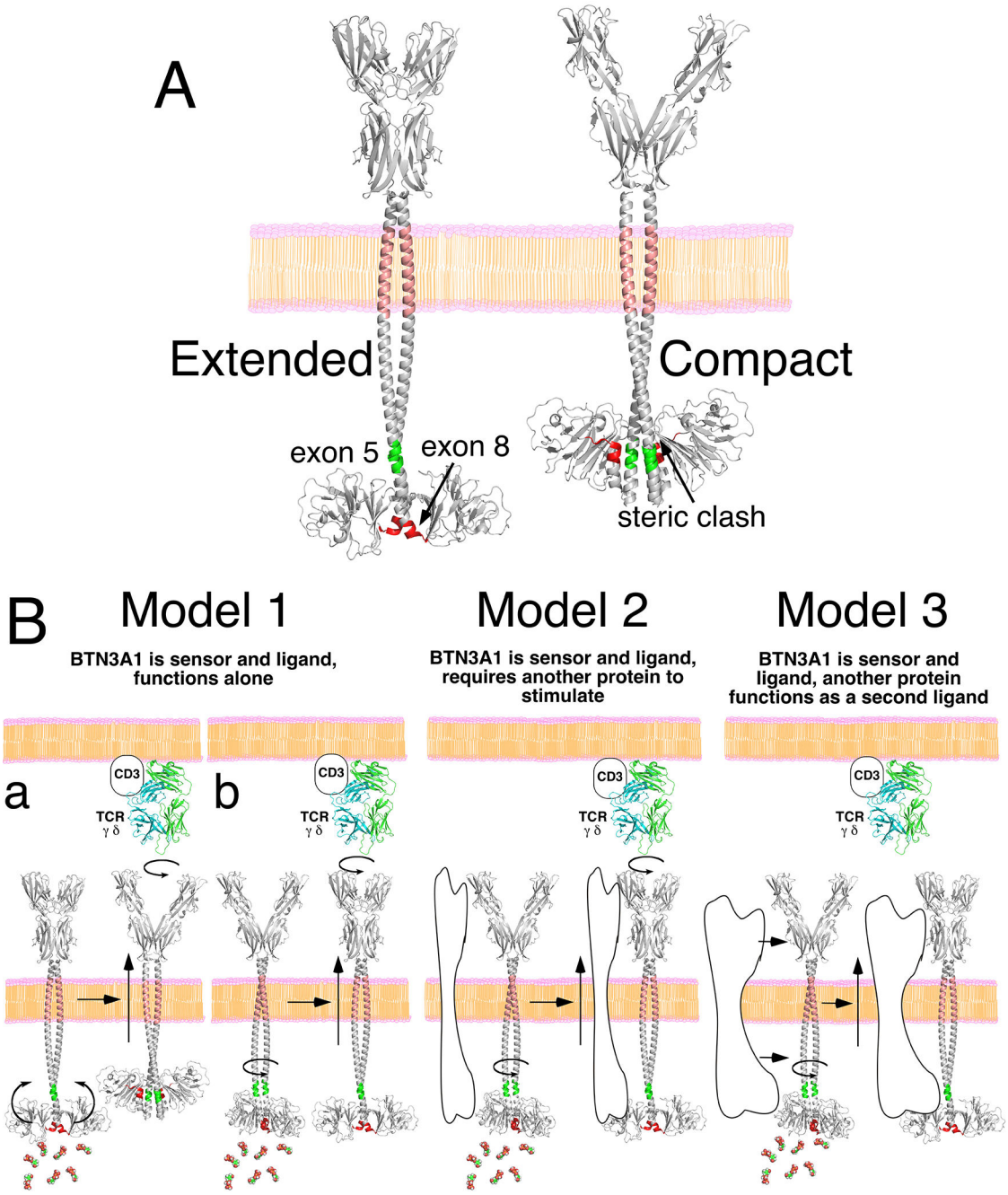

FIGURE 10.

Models for the structure of BTN3A1 and mechanism of its action. (**A**) Potential structure of BTN3A1 in an extended or a compact form. In the both models, the juxtamembrane region is shown as a coiled-coil dimer beginning immediately after the transmembrane segment and ending at residue 282 (extending to the end of exon 5 shown in green). For the extended model, the remainder of the α helix is from the extended B30.2 crystal structure (PDB 5HM7) and ends at exon 8 (shown in red) from the BTN3A1 B30.2 dimer (PDB 4V1P). For the compact model, 5HM7 B30.2 monomers were positioned at the ends of the coiled-coil segments. Note that there is a steric clash that results suggesting that if this structure exists,

the B30.2 domains would need to accommodate the α-helical regions. (**B**) In model 1, BTN3A1 functions as both the sensor and the ligand without requiring a second protein. Sensing of prenyl pyrophosphates leads to a conformational change in the extracellular domains of BTN3. This requires either major movement of the B30.2 domains with disruption of the coiled-coil dimer interface (model 1a) or only a minor shift (model 1b). In model 2, BTN3A1 functions as the sensor and the ligand as in model 1 but requires a second protein(s) to function. Again, sensing of prenyl pyrophosphates leads to a conformational change in the extracellular domains of BTN3. In model 3, BTN3A1 functions as the sensor for prenyl pyrophosphates and as a ligand. A second protein also functions as a ligand for the Vγ2Vδ2 TCR. Note that in all models, BTN3A2 and BTN3A3 enhance surface expression of BTN3A1 and allow for maximum stimulation of Vγ2Vδ2 T cells.

Table I.

Juxtamembrane segments of human and murine BTN and BTNL proteins

Human	Murine	Predicted domain structure					
		IgV	IgC	TM to B30.2 or end	CC[a]	CC length h/m	B30.2
BN3A1	-	+	+	69	+	38	+
BN3A3	-	+	+	69	+	38	+
BN3A2	-	+	+	63	+	38	−
BTN2A1	-	+	+	58	+	47	+
BTN2A2	BTN2A2	+	+	49/41	+	32/32	+
BTNL9	BTNL9	+	+	51/47	+	29/28	+
ERMAP	ERMAP	+	− (h) /+ (m)	61/61	+	49/49	+
-	BTNL1	+	+	69	+/−	41	+
-	BTNL4	+	+	70	+/−	42	+
-	BTNL6	+	+	68	+/−	40	+
BTNL3		+	+	29	−		+
BTNL8		+	+	30	−		+
BTN1A1	BTN1A1	+	+	34/34	−		+
BTNL10	BTNL10	+	+	16/28	−		− (h) /+ (m)
MOG	MOG	+	−	20/15	−		−
BTNL2	BTNL2	+ (×2)	+ (×2)	4/37	−		−

[a]Based on the sum of the predicted presence of coiled-coil (CC) segments by the MARCOIL v1.0 program; + = >40%; +/− = 15–40%; − = <15%; h, human; m, murine; TM, transmembrane.